

https://doi.org/10.1093/plcell/koae197 Advance access publication 4 July 2024

Research Article

A cargo sorting receptor mediates chloroplast protein trafficking through the secretory pathway

Jinling Liu, ^{1,†} Hong Chen, ^{1,†} Li Liu, ^{1,†} Xiangzhao Meng, ¹ Qianwen Liu, ¹ Qinyi Ye, ¹ Jiangqi Wen, ^{2,3} Tao Wang, ^{1,*} Jiangli Dong Xiangli Dong, ^{1,*}

The author responsible for distribution of materials integral to the findings presented in this article in accordance with the policy described in the Instructions for Authors (https://academic.oup.com/plcell/pages/General-Instructions) is: Jiangli Dong (dongjl@cau.edu.cn).

Abstract

Nucleus-encoded chloroplast proteins can be transported via the secretory pathway. The molecular mechanisms underlying the trafficking of chloroplast proteins between the intracellular compartments are largely unclear, and a cargo sorting receptor has not previously been identified in the secretory pathway. Here, we report a cargo sorting receptor that is specifically present in Viridiplantae and mediates the transport of cargo proteins to the chloroplast. Using a forward genetic analysis, we identified a gene encoding a transmembrane protein (MtTP930) in barrel medic (Medicago truncatula). Mutation of MtTP930 resulted in impaired chloroplast function and a dwarf phenotype. MtTP930 is highly expressed in the aerial parts of the plant and is localized to the endoplasmic reticulum (ER) exit sites and Golgi. MtTP930 contains typical cargo sorting receptor motifs, interacts with Sar1, Sec12, and Sec24, and participates in coat protein complex II vesicular transport. Importantly, MtTP930 can recognize the cargo proteins plastidial N-glycosylated nucleotide pyrophosphatase/phosphodiesterase (MtNPP) and α -carbonic anhydrase (MtCAH) in the ER and then transport them to the chloroplast via the secretory pathway. Mutation of a homolog of MtTP930 in Arabidopsis (Arabidopsis thaliana) resulted in a similar dwarf phenotype. Furthermore, MtNPP-GFP failed to localize to chloroplasts when transgenically expressed in Attp930 protoplasts, implying that these cargo sorting receptors are conserved in plants. These findings fill a gap in our understanding of the mechanism by which chloroplast proteins are sorted and transported via the secretory pathway.

Introduction

Chloroplasts are typical photosynthetic plant organelles descended from photosynthetic prokaryotic cells that were engulfed by their eukaryotic hosts. During coevolution, the genome of the endosymbionts greatly reduced in size, with approximately 95% of these genes being integrated into the host's nuclear genome. Coding products of the nuclear prokaryote-derived genes are synthesized in the cytoplasm and then transported to the chloroplast through the posttranslational transport pathway (Van Wijk and Baginsky 2011; Sibbald and Archibald 2020; Forsythe et al. 2021). These proteins usually contain an N-terminal transit peptide as a localization signal during the precursor stage, which can be recognized and delivered to the chloroplast surface by cytoplasmic molecular chaperones. Entry into chloroplasts is then mediated by translocon complexes in the outer envelope (TOC) and inner envelope (TIC). Precursor proteins are cleaved by stromal processing peptidases and undergo the final folding process to become functional proteins (Sjuts et al. 2017; Xu et al. 2021).

Recent research evidence suggests that many chloroplast proteins carry additional signal peptides that are directed toward the endoplasmic reticulum (ER). These ER-directed signal peptides enable the proteins to target chloroplasts through the secretory pathway (Radhamony and Theg 2006). One example is Arabidopsis (Arabidopsis thaliana) α -carbonic anhydrase (α -CA, CAH1), which has a predicted ER-targeting peptide at its

N-terminus and acts on the chloroplast stroma. CAH1 is retained in the ER and Golgi-like structures in the presence of the vesicular transport inhibitor brefeldin A (BFA; Villarejo et al. 2005). Rice (Oryza sativa) plastidial N-glycosylated nucleotide pyrophosphatase/ phosphodiesterase (NPP) is another chloroplast protein that is transported via the secretory pathway. OsNPP1 contains many N-glycosylation sites and a cleavable hydrophobic signal sequence. BFA treatment of OsNPP1-GFP-expressing cells blocked the accumulation of OsNPP1-GFP in chloroplasts (Nanjo et al. 2006). It also has been reported that other members in this family, such as OsNPP2 and OsNPP6, can be transported to chloroplasts via the secretory pathway (Kaneko et al. 2016). Rice α -amylase I-1 (AmyI-1) is another secreted chloroplast glycoprotein. Both the mutant forms of small GTPase ADP-ribosylation factor 1 (ARF1) and Secretion-associated and RAS-superfamily related 1 (Sar1), which impaired ER-to-Golgi vesicle transport, inhibited the plastid targeting of AmyI-1 (Chen et al. 2004; Asatsuma et al. 2005; Kitajima et al. 2009). These data suggest that in flowering plants, glycosylation-modified chloroplast proteins can be transported via the secretory pathway. However, the molecular mechanisms by which the secretory pathway sorts these chloroplast proteins with ER-directed signal peptides have remained elusive for a long time.

ER-synthesized secreted proteins are generally selected by coat protein complex II (COPII) and exported as membrane-bound

¹College of Biological Sciences, China Agricultural University, Beijing 100193, China

²Institute for Agricultural Biosciences, Oklahoma State University, Ardmore, OK 73401, USA

³Department of Plant and Soil Sciences, Oklahoma State University, Stillwater, OK 74078, USA

^{*}Author for correspondence: dongjl@cau.edu.cn (J.D.), wangt@cau.edu.cn (T.W.)

[†]These authors contributed equally to this work.

vesicles. Membrane proteins, as the transported substrates, can be wrapped directly into COPII vesicles, whereas the soluble proteins require transmembrane sorting receptors as intermediaries for vesicle incorporation. These transmembrane sorting receptors interact with both the cargo proteins and coat proteins to bind specific substrates and facilitate their incorporation into vesicles (Dancourt and Barlowe 2010). COPII is a functionally conserved series of proteins in eukaryotes. The ER-mediated COPII export process is initiated by the small GTPase Sar1, which is activated by the ER-localized transmembrane Sar1-specific guaninenucleotide exchange factor Sec12. Then the Sec23/24 complex is recruited from the cytoplasm, resulting in the formation of a preemergence complex. Subsequently, a cage-like lattice transport vesicle with a cuboctahedral shape is formed by recruitment of the heterologous tetramer of Sec13/31 via Sec23. After wrapping cargos into these transport vesicles, protein-sorting receptors release the bound substrates to the cis-Golgi or Golgi compartment and then recycle back to the ER for a new round of cargo export (Marti et al. 2010; Chung et al. 2016; Béthune and Wieland 2018; Weigel et al. 2021). Studies in mammals and yeasts have identified different types of cargo sorting receptors that recognize carbohydrate and/or peptide signals in secretions, including ER-Golgi intermediate compartment protein-53 (ERGIC-53), p24, and a range of ER vesicle proteins. These cargo sorting receptors recognize specific substrates and shuttle through the ER and Golgi apparatus via COPI/COPII vesicles (Dancourt and Barlowe 2010; Geva and Schuldiner 2014; Barlowe and Helenius 2016). A wellstudied cargo sorting receptor in plants is the p24 family protein. Similar to homologs in mammals and yeasts, the C-terminus of most plant p24 proteins contains a dilysine motif and a diaromatic motif, which interact with the COPI and COPII subunits, allowing p24 proteins to function effectively in the early secretory pathway (Contreras et al. 2004; Langhans et al. 2008; Montesinos et al. 2014). Most cargo sorting receptors in plant cells have been identified by homologous sequence comparison with the identified counterparts in yeasts and mammals. So far, cargo receptors that mediate the transport of chloroplast proteins through vesicles have not been identified in plants.

Here, we identified an ER exit site (ERES) and Golgi dual-localization protein, MtTP930, which functions as a chloroplast protein-sorting receptor in the ER. MtTP930 cooperates with Sar1, Sec12, and Sec24 to mediate the transport of the chloroplast proteins NPP and CAH through the COPII vesicle transport pathway. This kind of cargo sorting receptor is specifically present in green plants. Our results elucidate the molecular mechanisms of chloroplast protein transport via the secretory pathway.

Results

Identification of Mttp930 mutants

Chloroplasts are plant cell-specific energy-converting organelles and are essential for plant growth and development. To identify the genes that affect chloroplast function, we screened the the transposable element of *Nicotiana tabacum* cell type 1 (*Tnt1*) retrotransposon insertional mutant in *M. truncatula* mutant plants obtained from the Noble Research Institute (Cheng et al. 2011, 2014). We identified a mutant, NF15873, exhibiting a light leaf color and dwarf phenotype from the mutant population (Fig. 1A). Deep sequencing analysis of the NF15873 mutant revealed the presence of 47 *Tnt1* insertions within its genome (Supplementary Table S1). To further identify the gene responsible for the mutant phenotype, PCR amplification analysis was performed based on the

flanking sequences of Tnt1 insertion sites of the NF15873 (https://medicago-mutant.dasnr.okstate.edu/mutant/index.php; Fig. 1B). Comparison between the flanking sequence and the genomic sequence showed that Tnt1 was inserted in the first exon of Medtr7g095930 (Fig. 1A), which encodes a putative transmembrane protein of unknown function, henceforth referred to as MtTP930. Only a single copy of this gene was found in the M. truncatula genome database (https://medicago.toulouse.inra.fr/MtrunA17r5.0-ANR/).

Based on the coding sequence of MtTP930, we found 2 other mutants, NF18192 and NF7638, in which the Tnt1 insertions were identified in different loci of MtTP930 (Fig. 1, A and C). PCR-based genotyping showed that the phenotypes of all 3 of these mutants were associated with mutations in MtTP930. Comparison between the flanking sequences and the genomic sequence showed that in all the 3 mutants, the Tnt1 insertion occurred in the first exon region of MtTP930, located 103, 206, and 296 bp downstream of the start codon, respectively (Fig. 1A). Expression of MtTP930 was not detected in any of the 3 mutants by RT-PCR analysis (Fig. 1D). This indicates that the transcription expression of MtTP930 is lost due to the insertion of Tnt1, and the MtTP930 mutants are loss-of-function mutants.

Compared with the wild-type (WT) R108, the chlorophyll content (indicated by SPAD) of these 3 mutants was substantially reduced. Both the maximum quantum yield $F_{\rm v}/F_{\rm m}$ and the actual quantum yield Y(II) of the mutants were significantly lower than those of the WT (Fig. 1E). The light curves and fluorescence-induced kinetic curves of the mutants were lower than those of the WT as well (Fig. 1F). The length of the aerial part, root length, fresh weight of the aerial part, and fresh weight of the root were significantly reduced (Fig. 1G). These results suggest that the chloroplast function was impaired and the growth was inhibited in these 3 mutants.

To further confirm that the Tnt1 insertion in MtTP930 is responsible for the mutant phenotype, a fragment including the promoter and the coding sequence of MtTP930 was stably expressed in the NF15873 and NF18192 mutants, respectively. The phenotype of the Mttp930 mutants was fully complemented (Fig. 1, E to G). The chlorophyll content, maximum quantum yield $F_{\rm v}/F_{\rm m}$, and the actual quantum yield Y(II) were restored to the WT levels (Fig. 1E). The light curves and fluorescence-induced kinetic curves of MtTP930/Mttp930 complement plants showed no significant differences compared to the WT (Fig. 1F). The length of the aerial part, root length, fresh weight of the aerial part, and fresh weight of root were also rescued by MtTP930 expression in mutant plants (Fig. 1G). In conclusion, these data confirm that the loss of function of MtTP930 is responsible for the impaired chloroplast function and inhibition of plant growth in the mutants.

MtTP930 is highly expressed in the aerial parts and is widely present in Viridiplantae

RT-qPCR analysis showed that MtTP930 was relatively expressed at high levels in the aboveground parts of plants, especially in the leaves (Supplementary Fig. S1A). To further determine the expression pattern, we generated stable transgenic plants with a construct that incorporates the promoter region of MtTP930 driving the expression of the GUS reporter gene. GUS expression signal was detected in plant leaves and in vascular tissues, suggesting that MtTP930 mainly acts in the plant leaves (Supplementary Fig. S1B). The similar findings were obtained by immunoblotting of the GUS protein (Supplementary Fig. S1C). The results of amino acid sequence alignment and clustering analysis showed that the

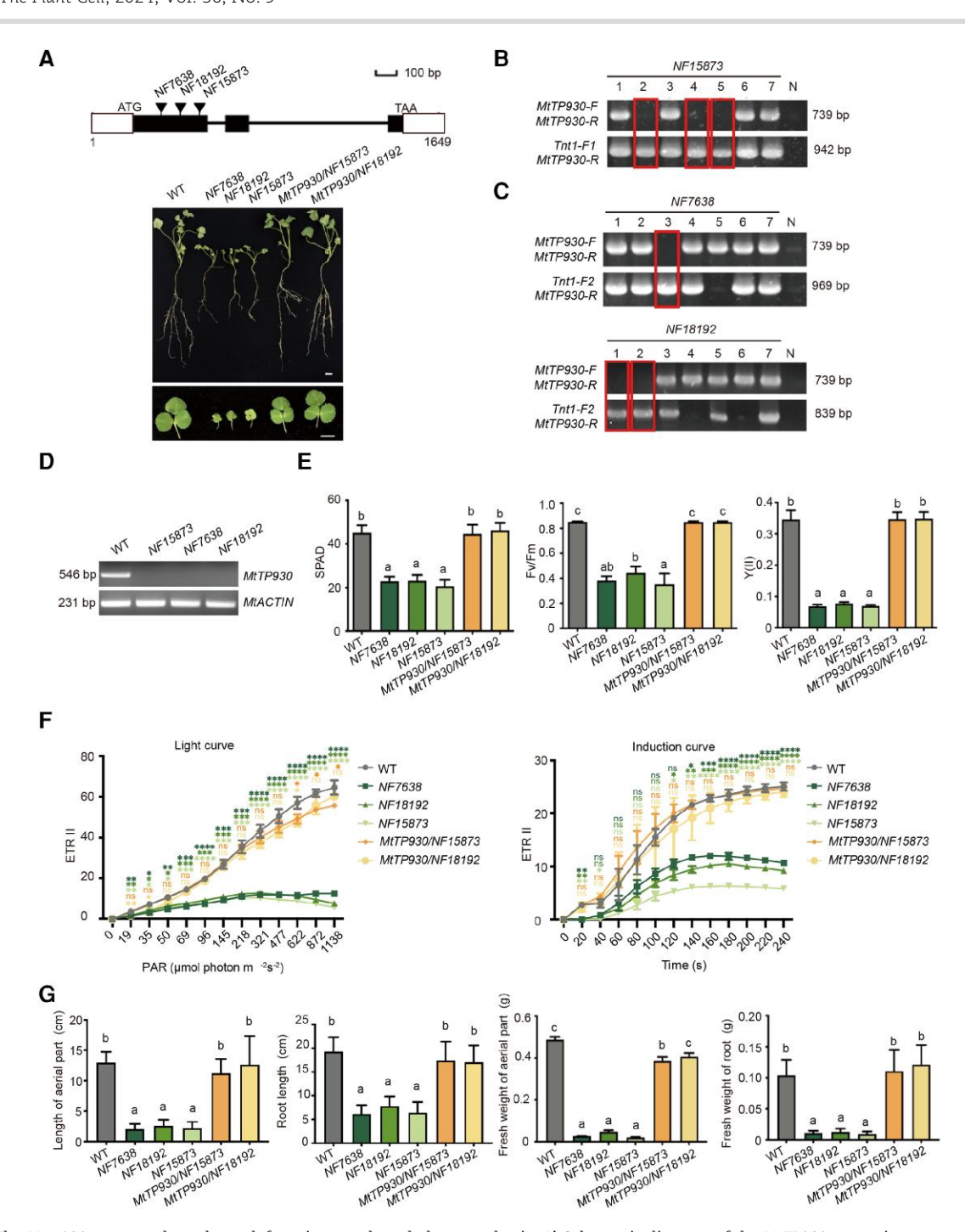


Figure 1. The Mttp930 mutant plants have defects in growth and photosynthesis. A) Schematic diagram of the MtTP930 genomic structure and Tnt1 insertion sites. Solid rectangles represent exons, hollow rectangles represent 5' or 3' UTR, and lines represent introns. The vertical arrow marks the location of Tnt1 retrotransposon in the Mttp930 mutants. Scale bar, 100 bp. WT, NF7638, NF18192, and NF15873 mutant plants and proMtTP930:MtTP930/ NF15873 and proMtTP930:MtTP930/NF18192 plants grown under normal conditions for 4 wk. Scale bar, 1 cm. B and C) PCR identification of the Mttp930 mutants. The Tnt1 insertion mutants of NF7638, NF18192, and NF15873 were identified. The templates were genomic DNA from the T1 generation isolated from the NF7638, NF18192, and NF15873 mutants. Tnt1-F1, Tnt1-F2, MtTP930-F, and MtTP930-R were primers for PCR of the extracted genomic DNA. The red box represents the NF7638, NF18192, and NF15873 Tnt1 homozygous mutants. N, negative control. D) RT-PCR analysis of full-length transcripts of MtTP930 in WT and NF7638, NF18192, and NF15873 mutant plants. MtACTIN was the internal reference gene. E) The chlorophyll content (SPAD indicated), maximum quantum yield (F_v/F_m) and actual quantum yield Y(II) of 4-wk-old WT, NF7638, NF18192, and NF15873 mutant plants and proMtTP930:MtTP930/NF15873 and proMtTP930:MtTP930/NF18192 plants. The data were expressed as mean \pm se. One-way ANOVA, $n \ge 30$; significant differences are labeled (a, b, c, P < 0.05). F) The light curves and fluorescence-induced kinetic curves of 4-wk-old WT, NF7638, NF18192, and NF15873 mutant plants and proMtTP930/NF15873 and proMtTP930/NF18192 plants. The data were expressed as mean ± st. One-way ANOVA, n = 2; significant differences are labeled (*P < 0.05, **P < 0.01, ***P < 0.001, ***P < 0.001, and ns, nonsignificant). ETR: relative electron transfer rate. Light curve: the light curve program exposes a sample to stepwise increasing intensities of actinic illumination. In "rapid light curves" (RLC), the time interval of each light step is short (down to 10 s) and full equilibration of photosynthetic reactions is not reached within an illumination interval. Light induction curve data obtained follow the typical "slow-phase" fluorescence induction kinetics. G) The length of aerial part, root length, fresh weight of aerial part, and fresh weight of root of the 4-wk-old WT, NF7638, NF18192, and NF15873 mutant plants and proMtTP930/MtTP930/NF15873 and proMtTP930/MtTP930/NF15873 and proMtTP930/MtTP930/NF15873 mutant plants and promtTP930/NF15873 and proMtTP930/NF15873 mutant plants and plants an NF18192 plants. The data were expressed as mean ± sɛ. One-way ANOVA, n≥15; significant differences are labeled (a, b, c, P < 0.05).

homologs of MtTP930 were widely present in Viridiplantae, including Chlorophyta (Chlamydomonas reinhardtii, Auxenochlorella protothecoides, etc.), Bryophyta (Marchantia polymorpha), Pteridophyta (Selaginella moellendorffii) and Angiospermae (Medicago truncatula, A. thaliana, Zea mays, etc.; Supplementary Fig. S2). All these plants obtain energy through photosynthesis; thus, all above results imply that these kinds of genes mainly associate with chloroplasts in green plants.

MtTP930 is involved in the COPII vesicular transport pathway

MtTP930 and its homologs are a class of transmembrane proteins unique to green plants, and the biological function of MtTP930 has not been reported. To further understand the function of MtTP930, we utilized the online tool "Phobius server" (a combined transmembrane topology and signal peptide predictor, https:// phobius.sbc.su.se/) to predict the topology of MtTP930, and the prediction result showed that MtTP930 has 2 transmembrane domains (Fig. 2A). To verify the predicted topology of MtTP930, we employed the plant cell component separation and the protease protection assay. We fused a Flag-tag to the C-terminus of the MtTP930 protein and utilized Agrobacterium tumefaciens injection to transiently express the fusion protein in Nicotiana benthamiana leaves. The nuclear, cytoplasmic, and membrane fractions were isolated from the plant leaves 3 d after transient expression, and the immunoblotting analysis showed that expression of the MtTP930 protein was solely detected in the membrane fraction (Fig. 2B). To further ascertain the orientation of the N- and C-termini of MtTP930 toward the ER lumen or cytoplasm, we conducted a protease protection assay employing isolated microsomes derived from N. benthamiana leaves expressing MtTP930-Flag. Following 2-h coincubation with trypsin, the MtTP930-Flag protein was nearly undetectable in the absence of Triton X-100, while the ER lumen marker protein BIP remained largely unaffected. Subsequently, when Triton X-100 was introduced to the reaction system, after a 2-h trypsin incubation, the membrane structure was disrupted, resulting in the degradation of both MtTP930-Flag and BIP (Fig. 2C). The result suggests that MtTP930-Flag is likely exposed to the cytoplasm. Protein structure analysis shows that MtTP930 has a double transmembrane domain and that the N-terminus locates in the same direction as the C-terminus (Fig. 2A), and protease protection experiments show that the C-terminus locates in the cytoplasm (Fig. 2C). These results clarify that MtTP930 is a double transmembrane protein with its N- and C-termini facing the cytoplasm (Fig. 2D).

To further determine where MtTP930 functions, we first analyzed the subcellular localization of MtTP930. The MtTP930-GFP expression vector was transiently expressed in N. benthamiana leaves by A. tumefaciens injection. The results indicated that MtTP930-GFP exhibited a punctate and reticulate distribution, with the punctate fluorescence appearing to be mobile (Supplementary Video S1). The above results speculate that MtTP930 is related to the secretory protein synthesis and organelle transport (Geldner et al. 2009; De Craene et al. 2014). To determine the detailed distribution of MtTP930, MtTP930-GFP was coexpressed with 2 subcellular specific markers, respectively. Sec12, a guanine-nucleotide exchange factor associated with the ER membrane, and GTPase Sar1, a secretion-associated Ras-associated protein 1, are 2 important proteins responsible for the assembly of COPII proteins in the ER (Bar-Peled and Raikhel 1997; Zeng et al. 2015). Confocal microscopy analysis revealed that MtTP930 colocalized with the ERES marker proteins Sar1 and Sec12 (Fig. 2E). To further determine the localization of the endogenous MtTP930 protein, MtTP930 small peptide antibody was used for immunofluorescence studies in M. truncatula. Given that MtTP930 is associated with vesicular transport, we opted to utilize 2 markers, the Golgi maker ARF1, which is involved in the COPI pathway, and the ERES marker Sar1. As a result, MtTP930 can be colocalized with the marker of ARF1 and Sar1 (Fig. 2F). Combined with the evidence of transient expression and in situ expression, it can be concluded that MtTP930 is localized in ERESs and Golgi.

To further determine whether MtTP930 is involved in the initiation of vesicle transport through direct interaction with Sec12. Sar1, and Sec24, we identified the homologs of these 3 proteins in M. truncatula (Fig. 3, A to C). To test the relation between MtTP930 and COPII proteins, we performed firefly luciferase complementation imaging assays in N. benthamiana leaves and confirmed that MtTP930 interacts with Sec12, Sar1, and Sec24 (Fig. 3, D to F). We verified these interactions by bimolecular fluorescence complementation (BiFC) in the protoplasts (Supplementary Fig. S3, A to C), split-ubiquitin yeast 2-hybrid (SuY2H, to test protein-protein interactions of transmembrane proteins; Supplementary Fig. S3, D and E), and coimmunoprecipitation (Co-IP) assays in A. thaliana protoplasts or N. benthamiana leaf cells (Fig. 3, G to I). Together, these results suggest that MtTP930 can be involved in the COPII vesicle transport pathway and function in the initiation phase.

MtTP930 acts as a cargo sorting receptor of the COPII pathway

Amino acid sequence analysis of MtTP930 protein showed that MtTP930 has a tripeptide (PPP) motif and a dilysine (KK) motif (Fig. 4A; Supplementary Table S2). The PPP motif has been reported to bind to a range of COPII proteins in mammals, while the KK motif, a specific cargo sorting receptor sequence reported in mammals, plants, and yeast, can bind to COPI proteins and mediate retrograde transport from the Golgi apparatus to the ER (Contreras et al. 2004; Dancourt and Barlowe 2010; Peotter et al. 2019; Raote et al. 2020). To demonstrate whether MtTP930 is a cargo sorting receptor, we deleted the motifs and detected the location of the 3 mutant forms of MtTP930 (MtTP930 $^{\triangle PPP}$, MtTP930 $^{\triangle KK}$, and MtTP930 $^{\triangle PPP\ KK}$). Then, we investigated the effect of the PPP and KK mutation on the MtTP930 by colocalization analysis with Sar1-GFP (ERES marker) and GFP-SYP32 (Golgi marker), respectively. The result showed that the 3 mutant forms of MtTP930 were colocalized with Sar1-GFP, but no longer colocalized with the GFP-SYP32 (Fig. 4, B and C). The mutations within the PPP or KK motifs were likely to alter the functionality of MtTP930, impeding its efficient movement through the secretory pathway and disrupting its crucial role in cargo sorting. Therefore, these findings imply that the mutations are directly responsible for the retention of MtTP930 at the ERESs and the subsequent impairment of its function as a cargo sorting receptor.

MtTP930 mediates vesicle transport of chloroplast proteins MtNPP and MtCAH

Based on the above results, we found that MtTP930 acts as a cargo sorting receptor in the COPII vesicle transport pathway, and mutations of MtTP930 directly affect the function of plant chloroplasts. Evidence suggests that the secretory pathway can be involved in the transport of nuclear-encoded chloroplast proteins (Villarejo et al. 2005; Nanjo et al. 2006; Radhamony and Theg 2006). Therefore, we hypothesized that MtTP930 could act as a

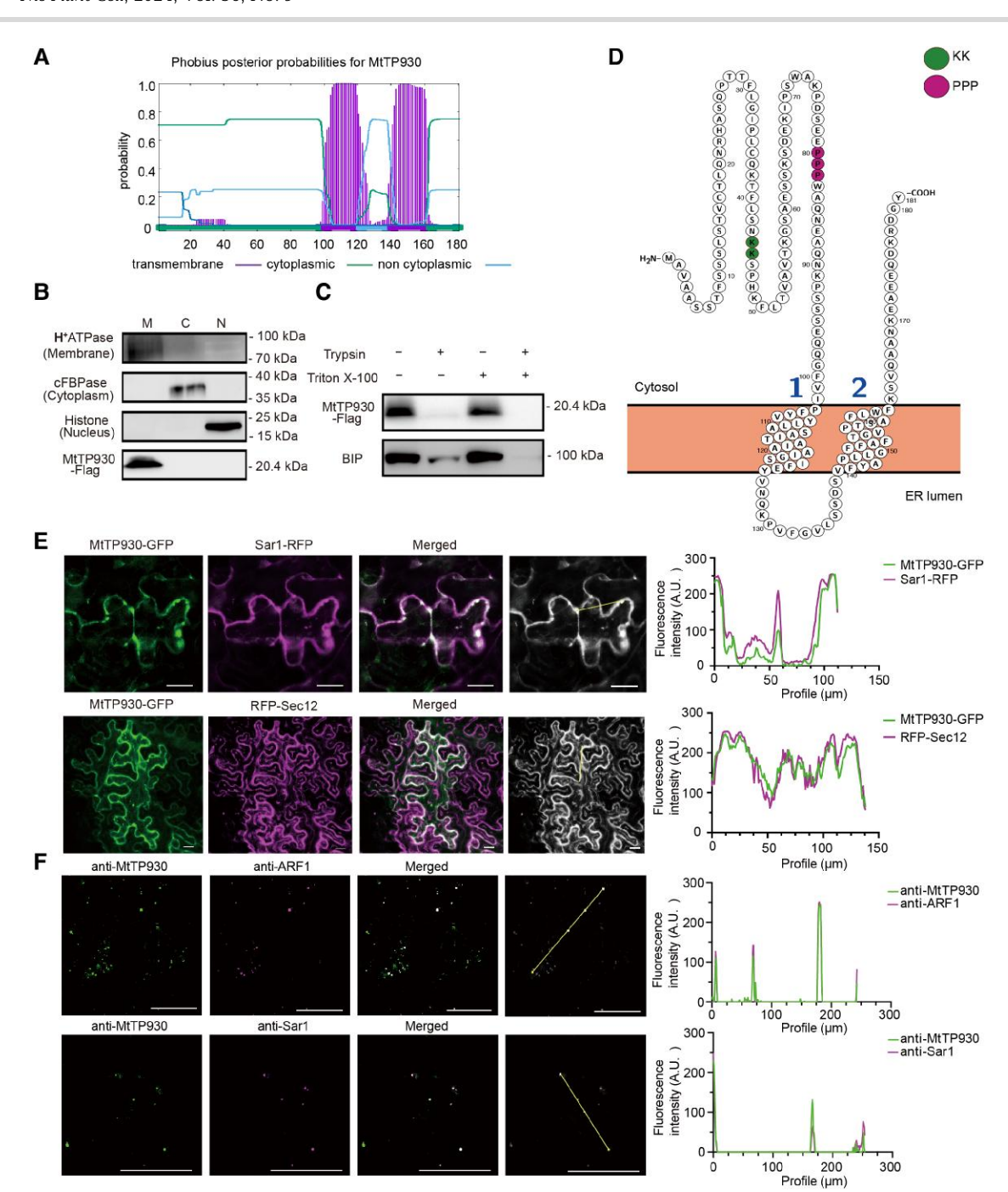


Figure 2. MtTP930 was a dual-localization protein at ERESs and Golgi. A) The hypothetical membrane topology of MtTP930 predicted by the online tool "Phobius server" (https://phobius.sbc.su.se/). B) Cellular fractionation and immunoblotting analysis of MtTP930-Flag protein in N. benthamiana leaves. M, membrane proteins; C, cytoplasmic proteins; N, nuclear proteins. Immunoblotting analysis with Flag, H+-ATPase (membrane marker), cFBPase (cytoplasmic marker), and Histone (nuclear marker) antibodies. C) Protease protection assay on the topology of MtTP930. MtTP930-Flag was expressed in N. benthamiana leaves. Microsomes were isolated and treated with (+) or without (-) trypsin and with (+) or without (-) Triton X-100. Immunoblotting analysis with Flag and BIP antibody, respectively. ER lumen protein BIP as control. D) Proposed topology of MtTP930, revised from the "Protter" (http:// wlab.ethz.ch/protter/). E) Colocalization of MtTP930-GFP, Sar1-RFP, and RFP-Sec12 in N. benthamiana leaf cells. Monitored by SP8 laser scanning confocal system. This far right panel converted the merge graph from RGB format to 8-bit format in order to make the straight lines appear more clearly. The relative fluorescence intensities shown were measured using the ImageJ software. The horizontal axis represents the pixel points on the line, and the vertical axis is the corresponding grayscale value of each point; the image represents the trend of the grayscale change. Comparison of the GFP/RFP channel results reflected the colocalization situation. Scale bar, 20 µm. F) Localization of MtTP930 in M. truncatula root cells by immunofluorescence assay. Detected by corresponding antibodies (anti-MtTP930, anti-ARF1, and anti-Sar1). Monitored by SP8 laser scanning confocal system. Scale bar, 20

cargo sorting receptor for nucleus-encoded chloroplast proteins, mediating trafficking of these chloroplast-targeted proteins. OsNPP1 is a nucleus-encoded chloroplast protein that is transported via the secretory pathway (Nanjo et al. 2006). MtNPP was identified in M. truncatula by homologous protein sequence comparison (Fig. 5A). A previous study reported that OsNPP1 is a secreted glycoprotein (Nanjo et al. 2006). We analyzed the amino acid sequence of MtNPP and predicted 7 putative N-glycosylation sites from the NetNGlyc website (https://services.healthtech.dtu. dk/services/NetNGlyc-1.0/; Supplementary Fig. S4). To investigate

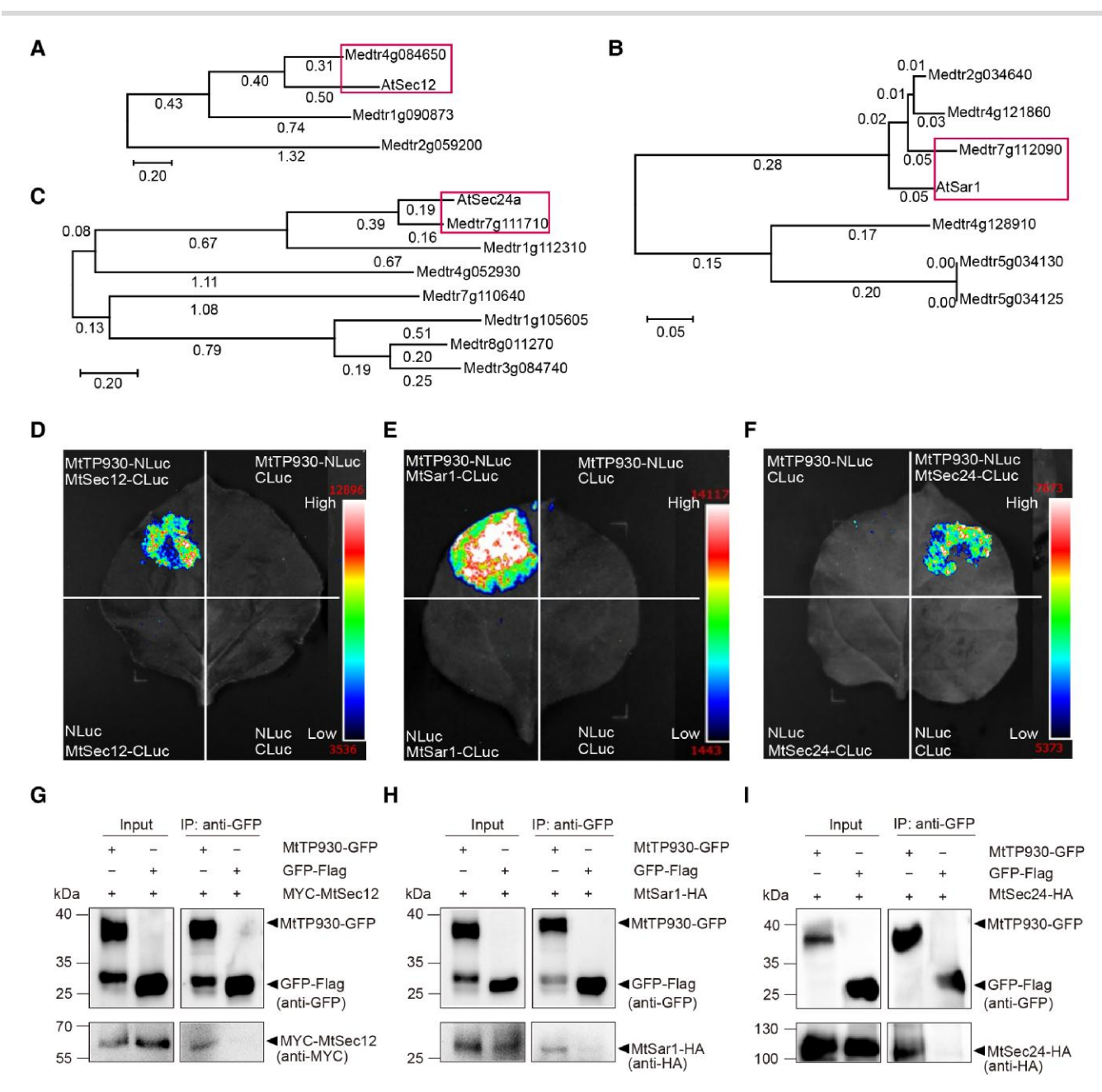


Figure 3. MtTP930 interacted with COPII proteins. A to C) Phylogenetic identification of the homologs of AtSec12, AtSar1, and AtSec24 in M. truncatula genomic database through BLAST search (https://medicago.toulouse.inra.fr/MtrunA17r5.0-ANR/). The tree is drawn to scale, with branch lengths (next to the branches) in the same units as those of the evolutionary distances used to infer the phylogenetic tree. The box marked Medtr4g084650 is MtSec12, Medtr7g112090 is MtSar1, and Medtr7g111710 is MtSec24. D to F) Firefly luciferase complementation imaging assays of the interaction between MtTP930 and MtSec12, MtSar1, and MtSec24 in N. benthamiana leaves. Luciferase fluorescence was detected using a CCD camera. The color scale represents the intensity of luminescence. G and H) Detection of the interaction between MtTP930 and MtSec12 or MtSar1 proteins by Co-IP in Arabidopsis protoplasts. MtTP930 was tagged with GFP (MtTP930-GFP). GFP-Flag was employed as the negative control. Total proteins were extracted from the Arabidopsis protoplasts, which were cotransformed with the indicated constructs and incubated with GFP beads to immunoprecipitate the target protein. Coprecipitated proteins were analyzed by immunoblotting using anti-GFP, anti-HA, and anti-MYC antibodies. I) Detection of the interaction between MtTP930 and MtSec24 proteins by Co-IP in N. benthamiana leaves. MtTP930 was tagged with GFP (MtTP930-GFP). GFP-Flag was employed as the negative control. Total proteins were extracted from the N. benthamiana leaves, which were cotransformed with the indicated constructs and incubated with GFP beads to immunoprecipitate the target protein. Coprecipitated proteins were analyzed by immunoblotting using anti-GFP and anti-HA antibodies.

whether MtNPP reaches chloroplasts via the secretory pathway, we used *N. benthamiana* protoplasts to study the localization pattern of MtNPP-GFP before and after BFA treatment. Subcellular localization analysis showed that MtNPP-GFP was localized in chloroplasts (Fig. 5B). Under BFA treatment, MtNPP-GFP was not localized in chloroplasts (Fig. 5B), similar to the retention of OsNPP in the ER and Golgi-like region under BFA treatment

(Nanjo et al. 2006). The domain inactivated forms of ARF^{T31N}-RFP and Sar^{H74L}-RFP inhibit vesicle transport from the ER to the Golgi apparatus in Arabidopsis (Takeuchi et al. 2000; Stefano et al. 2006). Thus, we cotransferred MtNPP-GFP with ARF^{T31N}-RFP and Sar^{H74L}-RFP into N. benthamiana protoplasts, respectively, and analyzed the alterations in the localization pattern of MtNPP-GFP. The results showed that MtNPP-GFP exhibited a

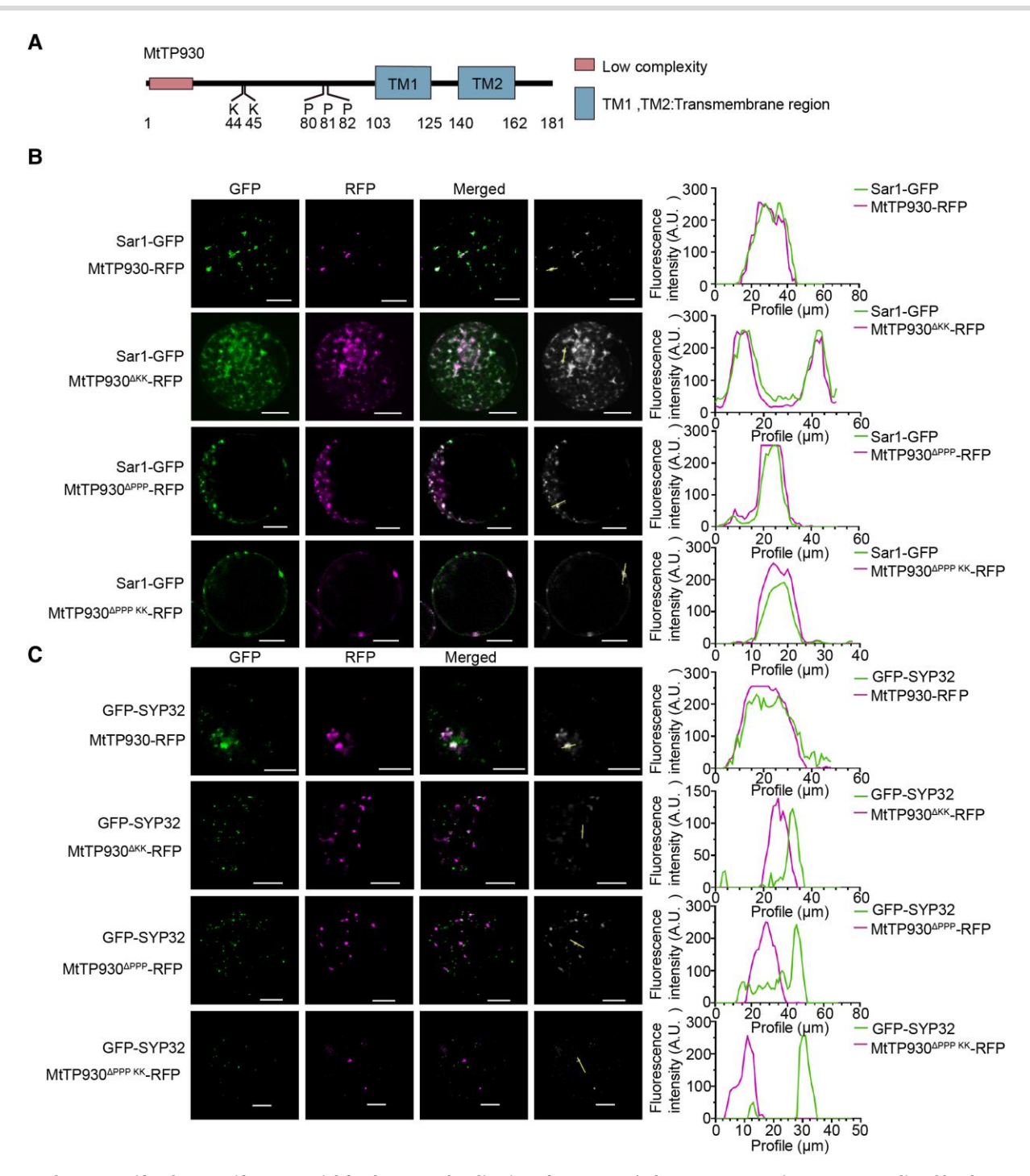


Figure 4. The PPP motif and KK motif are essential for the proper localization of MtTP930. A) The MtTP930 protein structure predicted by the SMART website (https://smart.embl.de/; MtTP930, 1 to 181 aa). B) Cotransformed MtTP930 \triangle ^{KK}-RFP, MtTP930 \triangle ^{PPP}-RFP, or MtTP930 \triangle ^{PPP}-RFP with Sar1-GFP in N. benthamiana protoplasts. Scale bar, 20 μ m. **C)** Cotransformed MtTP930 $^{\triangle$ RFP, MtTP930 $^{\triangle}$ PPP-RFP, or MtTP930 $^{\triangle}$ PPP with GFP-SYP32 in N. benthamiana protoplasts. Scale bar, 20 μ m.

punctate distribution (Fig. 5B). The above results indicate that MtNPP is a glycosylation-modified protein and is transported to chloroplasts via the secretory pathway.

To further support our conclusion that MtTP930 is involved in the transport of MtNPP via the secretory pathway as a cargo sorting receptor, we analyzed the localization of MtNPP-GFP in WT and Mttp930 protoplasts. The results showed that MtNPP-GFP was localized in chloroplasts in the WT protoplasts, but MtNPP-GFP was distributed in a punctate pattern in the Mttp930 mutant protoplasts, which was similar to the results of

MtNPP-GFP localization after treatment with BFA (Fig. 5C). These results suggested that MtNPP is a cargo protein of MtTP930. To resolve whether MtTP930 acts as a cargo sorting receptor to directly bind MtNPP, we performed firefly luciferase complementation imaging assays and found that MtTP930 interacts with MtNPP (Fig. 5D), which was also determined by SuY2H and Co-IP assays (Fig. 5, E and F).

To further investigate the effect of the mutation of MtTP930 on MtNPP in vivo, we generated the stable transgenic plants expressing proMtNPP:MtNPP-GFP in the genetic background of the WT or

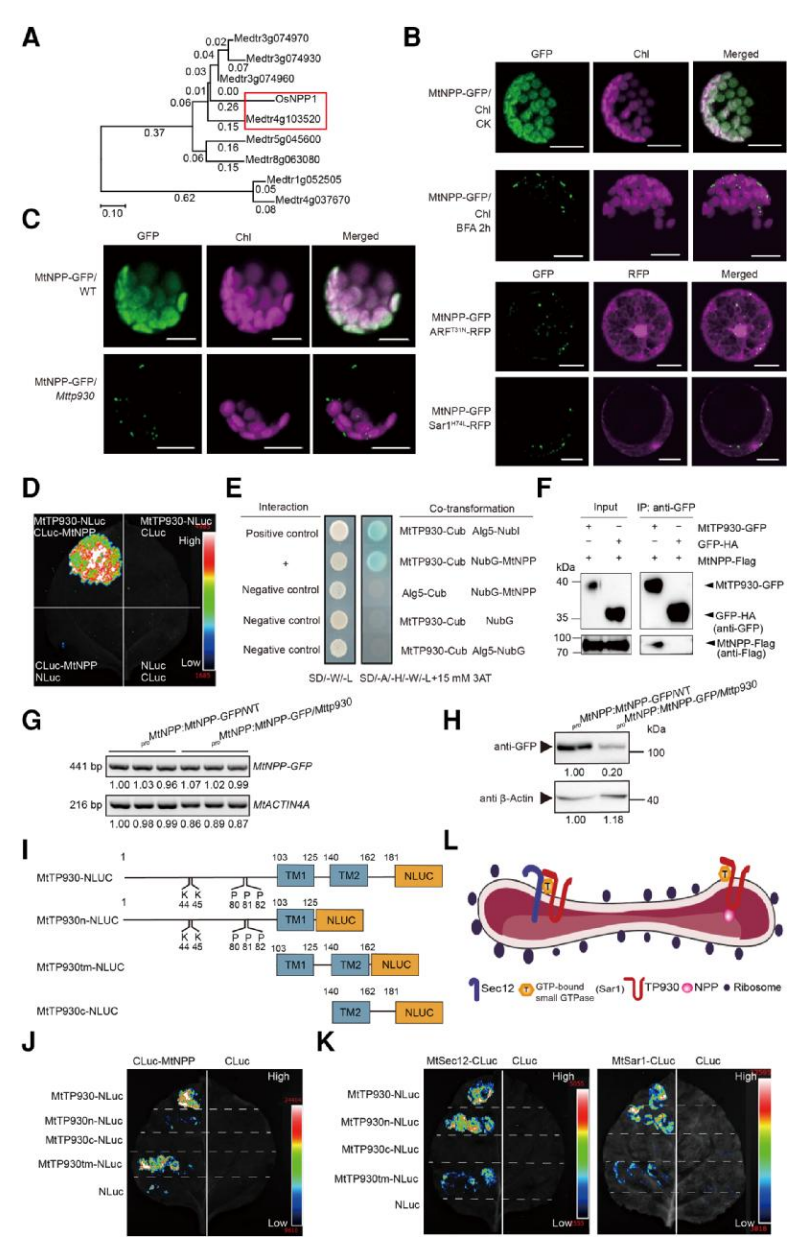


Figure 5. MtTP930 was responsible for MtNPP transporting from ER to Golgi. A) Identification of OsNPP1 homolog in M. truncatula by phylogenetic analysis through BLAST search (https://medicago.toulouse.inra.fr/MtrunA17r5.0-ANR/). The tree is drawn to scale, with branch lengths (next to the branches) in the same units as those of the evolutionary distances used to infer the phylogenetic tree. The box marked Medtr4g103520 is MtNPP. B) Subcellular localization of MtNPP before and after BFA treatment (BFA, 2 h). Coexpression of MtNPP-GFP with ARF^{T31N}-RFP or Sar1^{H74L}-RFP in N. benthamiana protoplasts, after 16-h incubation; MtNPP-GFP expressed protoplasts were treated with or without 10 µg/mL BFA for 2 h, then monitored by SP8 laser scanning confocal system. Chl is chloroplast autofluorescence. Scale bar, 20 µm. C) Effect of MtTP930 mutation on the chloroplast localization of MtNPP-GFP. Expression of MtNPP-GFP in WT and Mttp930 mutant protoplasts. After 16-h incubation, MtNPP-GFP was monitored by SP8 laser scanning confocal system. Chl is chloroplast autofluorescence. Scale bar, 10 µm. D) Firefly luciferase complementary imaging assays of the interaction of full-length MtTP930 and MtNPP proteins in N. benthamiana leaves. Luciferase fluorescence was detected using a CCD camera. The color scale represents the intensity of luminescence. E) SuY2H analysis of the interaction between MtTP930 and MtNPP. NMY51 yeast cells carrying the ADE2 and HIS3 reporter genes. Yeast cells were grown on an appropriate medium (which did not contain the indicated amino acids [A, Ade; H, His, W, Trp; L, Leu] but contained 15 mm 3-AT). Alg5-NubI with MtTP930-Cub was used as positive control, and Alg5-NubG with MtTP930-Cub and Alg5-Cub with NubG-MtNPP were used as negative controls, respectively. F) Detection of MtTP930 and MtNPP interaction by Co-IP. MtTP930 was tagged with GFP (MtTP930-GFP). MtNPP was tagged with Flag (MtNPP-Flag). GFP-HA was employed as the negative control. Total proteins were extracted from Arabidopsis protoplasts, which were cotransformed with the indicated constructs and incubated with GFP beads to immunoprecipitate the target protein. Coprecipitated proteins were analyzed by immunoblotting using anti-GFP and anti-Flag antibodies. G) RT-PCR analysis of transcripts of MtNPP-GFP in proMtNPP: MtNPP-GFP/WT and proMtNPP-GFP/Mttp930 plants. MtACTIN4A was employed for quantification. H) Immunoblot analysis of MtNPP-GFP in proMtNPP:MtNPP-GFP/WT and proMtNPP:MtNPP-GFP/Mttp930 plants. The MtNPP-GFP fusion protein driven by the native promoter of MtNPP (2 kb) was transferred into WT and Mttp930 mutant plants, and total proteins were extracted. β-Actin was employed for quantification. I) Schemes of full length or truncated forms of MtTP930 (MtTP930n, 1 to 125 aa; MtTP930tm, 103 to 162 aa; MtTP930c, 140 to 181aa). The MtTP930 protein structure predicted by the SMART website (https://smart.embl.de/). J) Firefly luciferase complementation imaging analysis of the interaction regions of MtTP930 with MtNPP in N. benthamiana leaves. Luciferase fluorescence was detected using a CCD camera. The color scale represents the intensity of luminescence. K) Firefly luciferase complementation imaging analysis of the interaction regions of MtTP930 with MtSec12 or MtSar1 in N. benthamiana leaves. Luciferase fluorescence was detected using a CCD camera. L) Schematic diagram of the inferred structural relationship between MtTP930 and MtSec12, MtSar1, and MtNPP on the ER based on their interaction relationship.

the Mttp930 mutants. RT-PCR analysis showed that transcript levels of MtNPP-GFP were consistent in proMtNPP:MtNPP-GFP/WT and proMtNPP:MtNPP-GFP/Mttp930 plants (Fig. 5G). Total proteins were extracted from proMtNPP:MtNPP-GFP/WT and proMtNPP: MtNPP-GFP/Mttp930 plants, and the quantitative immunoblotting results indicated that the protein content of MtNPP-GFP in proMtNPP:MtNPP-GFP/Mttp930 was lower than that in proMtNPP: MtNPP-GFP/WT plants (Fig. 5H). In conclusion, MtTP930 is involved in the secretory pathway transport of MtNPP as a cargo sorting receptor.

To delve deeper into the interaction regions of MtTP930 with MtNPP, MtSar1, and MtSec12, we truncated the MtTP930 protein into 3 segments: MtTP930n (comprising amino acids 1 to 125), MtTP930tm (103 to 162 aa), and MtTP930c (140 to 181 aa; Fig. 5I). These truncations were carefully chosen based on secondary structure analysis. Subsequently, firefly luciferase complementary imaging experiments were conducted to verify the interaction regions. The results showed that MtNPP could interact with fulllength MtTP930 and MtTP930tm, but did not interact with MtTP930n and MtTP930c, indicating that MtTP930 interacted with MtNPP through its luminal regions of the ER (Fig. 5J). In addition, MtSec12 or MtSar1 can interact with full-length MtTP930 and MtTP930n (Fig. 5K). The above results indicate that MtTP930 acts as a cargo sorting receptor, binds to MtNPP through its ER lumen region, and transports MtNPP through vesicles to the Golgi through its N-terminal interaction with COPII proteins (Fig. 5L).

We hypothesize that the cargos transported by MtTP930 are not limited to MtNPP. Several nuclear-encoded chloroplast proteins, including OsNPP1, OsNPP2, OsNPP6, OsAmyI-1, and AtCAH1, have been reported to be transported via the secretory pathway, which are N-glycosylated soluble proteins (Villarejo et al. 2005; Nanjo et al. 2006; Kitajima et al. 2009; Kaneko et al. 2016). We identified another chloroplast protein MtCAH by sequence alignment and evolutionary tree analysis in M. truncatula (Fig. 6A). We found that MtCAH has 3 putative N-glycosylation sites predicted by the NetNGlyc website (https://services.healthtech.dtu.dk/services/ NetNGlyc-1.0/; Supplementary Fig. S4). The subcellular localization in N. benthamiana protoplasts showed that MtCAH-GFP was localized in chloroplasts under normal conditions, but was not localized in chloroplasts after BFA treatment for 2 h (Fig. 6B). In the Mttp930 mutant, MtCAH-GFP was not localized in chloroplasts either (Fig. 6C) and may be localized in the vacuole. MtTP930 can also directly interact with MtCAH by firefly luciferase complementation imaging assay in N. benthamiana leaves and SuY2H analysis (Fig. 6, D and E). These results showed that MtTP930 as a cargo sorting receptor is also involved in the translocation of another chloroplast protein MtCAH.

In conclusion, MtTP930 acts as a cargo sorting receptor, mediating cargo proteins MtNPP and MtCAH trafficking to chloroplasts via the vesicular transport pathway. It deserves further study whether there are other cargo sorting receptor proteins that transport MtNPP and MtCAH into chloroplasts via the vesicular transport pathway. In addition, whether MtTP930 exclusively facilitates the transport of chloroplast proteins needs to be further investigated.

The function of TP930 is conserved

To further demonstrate the widespread occurrence of TP930 function in plants, we identified the homologous gene At3g51510 (AtTP930) in Arabidopsis by BLAST and phylogenetic analysis (Supplementary Fig. S5A). RT-qPCR analysis in different tissues of Arabidopsis showed that AtTP930 exhibited high expression in the rosette leaf and cauline leaf, similar to that observed in

M. truncatula (Supplementary Fig. S5B). We selected 2 target sites at the first exon of the AtTP930 gene and generated mutant plants using CRISPR/Cas9 in the Col-0 genetic background. Three mutant plants, line2, line3, and line5, with large deletions (-188, -110, and -45 bp, respectively) at the target gene were selected for further experiments (Supplementary Fig. S5C). The translation of AtTP930 is terminated prematurely in line2, and the start codons of line3 and line5 are missing. The T₂ generation plants of 3 mutant lines were used for phenotypic analysis. The results showed that the Attp930 mutant plants exhibited a chlorotic and dwarf phenotype, similar to that of Mttp930 mutant plants (Fig. 7, A, B, F, and G). The chlorophyll content of the Attp930 mutant plants was significantly reduced compared to that of the WT (Col-0; Fig. 7C). The maximum quantum yield F_v/F_m was significantly lower than that of the WT as well (Fig. 7, D and E). In addition, the primary root length and lateral root number of the mutant plants were significantly reduced compared with Col-0 plants (Supplementary Fig. S5, D to F). These results suggest that the Arabidopsis mutant plants have impaired chloroplast function and stunted growth, which is consistent with the phenotypes of the Mttp930 mutant. pE3025-MtNPP-GFP was transformed into Col-0 and Attp930 protoplasts, respectively. MtNPP-GFP was localized in chloroplasts in the Col-0 protoplasts, but in the Attp930 mutant protoplasts, MtNPP-GFP was distributed in a punctate pattern (Fig. 7H), similar to that in M. truncatula. Combined with polygenetic tree analysis (Supplementary Fig. S2), MtTP930 and its homologs are conserved in green plants, and the mechanism by which this type of proteins function as cargo sorting receptors involved in trafficking of chloroplast proteins could be universal in green plants.

Discussion

Almost all chloroplasts in photosynthetic eukaryotes are derived from a single endosymbiotic event. Genes from endosymbionts are transferred into the host nuclear genome, and the nuclearencoded chloroplast proteins are synthesized in the cytoplasm and transported to the chloroplast by a posttranslational transport mechanism (Sibbald and Archibald 2020; Forsythe et al. 2021). Some chloroplast proteins in flowering plants are transported via the secretory pathway and require N-glycosylation modifications before entering the chloroplast (Villarejo et al. 2005; Nanjo et al. 2006; Kitajima et al. 2009; Kaneko et al. 2016). COPII vesicles transport newly synthesized cargo proteins and membrane lipids from the ER to the Golgi apparatus, while COPI vesicles mediate transport from the Golgi apparatus back to the ER (Béthune and Wieland 2018). In this study, we identified an ERES and Golgi dual-localized protein, MtTP930 (Fig. 2), that interacts with Sar1, Sec12, and Sec24 and participates in COPII vesicular transport (Figs. 3 and 4; Supplementary Fig. S3). In addition, the nuclear-encoded chloroplast proteins MtNPP and MtCAH are the cargos of MtTP930 in the secretory pathway, and these proteins did not reach the chloroplast in the Mttp930 mutants (Figs. 5 and 6). Therefore, MtTP930 is a cargo sorting receptor involved in chloroplast protein transport via the secretory pathway. Based on these findings, we derived a working model for the role of MtTP930 in the COPII pathway. MtTP930 localizes in the ERESs, it binds the cargo protein MtNPP or MtCAH in the ER lumen region, and it binds Sec12 through the N-terminus of its protein. Sar1 (a small GTPase) is locally activated and exposes hydrophobic structures through GDP-GTP exchange. Sar1 inserts into the ER membrane, after it was catalyzed by a guanine-nucleotide exchange factor (Sec12). Then the activated Sar1 recruits the inner coat protein Sec23/24, and inner coat proteins further recruit the outer

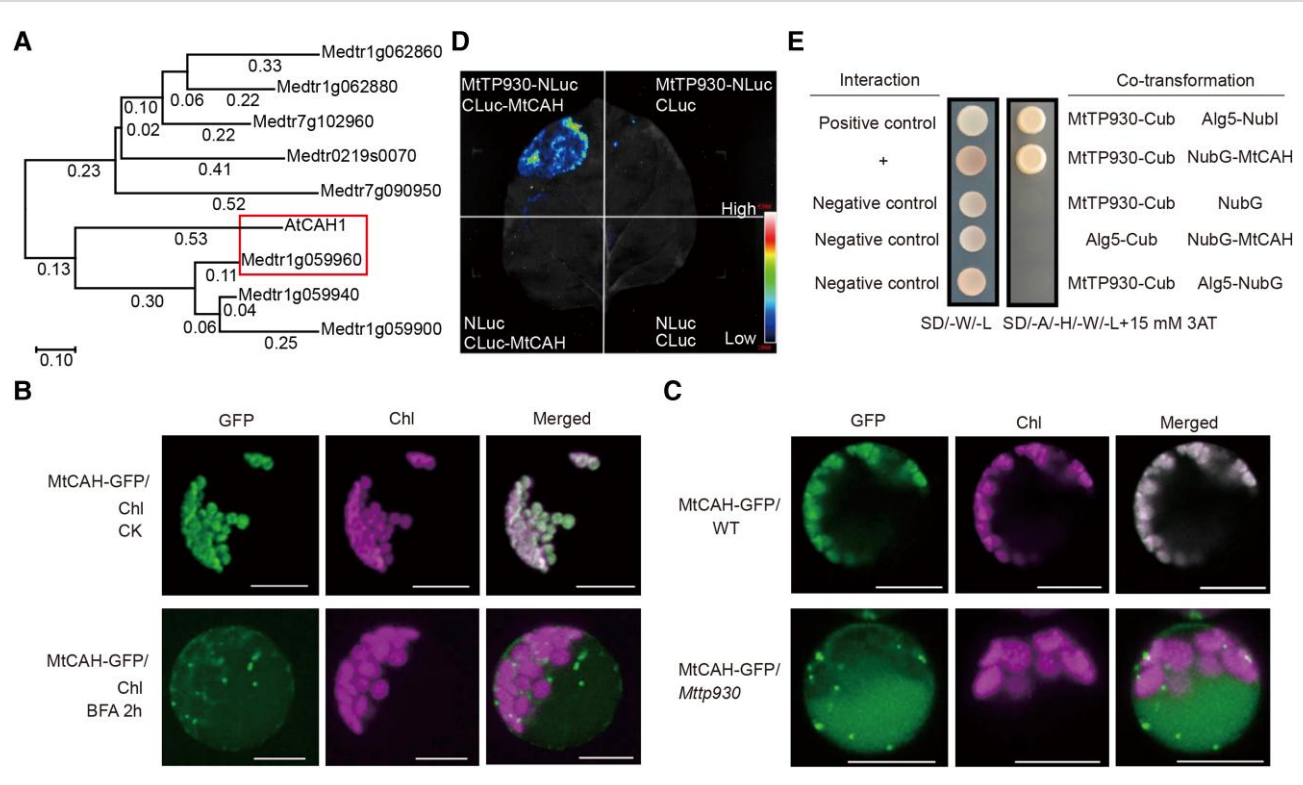


Figure 6. The localization of MtCAH was changed in Mttp930 mutant. A) Phylogenetic identification of AtCAH1 homolog in M. truncatula through BLAST search (https://medicago.toulouse.inra.fr/MtrunA17r5.0-ANR/). The tree is drawn to scale, with branch lengths (next to the branches) in the same units as those of the evolutionary distances used to infer the phylogenetic tree. The box marked Medtr1g059960 is MtCAH. B) Subcellular localization study of MtCAH before and after BFA treatment (BFA, 2 h). Expression of MtCAH-GFP in N. benthamiana protoplasts, after 16-h incubation; protoplasts were treated with or without 10 μ g/mL BFA for 2 h, then monitored by SP8 laser scanning confocal system. Chl is chloroplast autofluorescence. Scale bar, 20 μ m. C) Effect of MtTP930 mutation on the chloroplast localization of MtCAH-GFP. Expression of MtCAH-GFP in WT and Mttp protoplasts. After 16-h incubation, expression of MtCAH-GFP was monitored by SP8 laser scanning confocal system. Chl is chloroplast autofluorescence. Scale bar, 10 μ m. D) Firefly luciferase complementation imaging analysis of the interaction between full-length MtTP930 and MtCAH proteins in N. benthamiana leaves. Luciferase fluorescence was detected using a CCD camera. The color scale represents the intensity of luminescence. E) SuY2H analysis of the interaction between MtTP930 and MtCAH. NMY51 yeast cells carrying the ADE2 and HIS3 reporter genes. Yeast cells were grown on the appropriate medium (which did not contain the indicated amino acids [A, Ade; H, His, W, Trp; L, Leu] but contained 15 mm 3-AT). Alg5-NubI with MtTP930-Cub was used as the positive control, and Alg5-NubG with MtTP930-Cub and Alg5-Cub with NubG-MtCAH were used as negative controls, respectively.

coat proteins Sec13/31 to form the COPII assembly (Béthune and Wieland 2018). The cargo proteins are loaded into COPII vesicles and transported to the Golgi apparatus (Fig. 8).

The N-terminus of MtTP930 is necessary for its interaction with MtSar1 and MtSec12 (Fig. 5, I to L). The 2 motifs, KK and PPP, are also located on the N-terminus of MtTP930, which is of great significance for the functionality of MtTP930 (Fig. 4). Based on the above results, we speculated that the N-terminal fusion GFP tag might affect the function of MtTP930. We thus chose to fuse the GFP tag protein at the C-terminus of MtTP930 for subcellular localization study. To prove the functionality of the fluorescent fusion protein MtTP930-GFP, we generated the proMtTP930: MtTP930-GFP/Mttp930 complemented plants by stable genetic transformation. Expression of proMtTP930:MtTP930-GFP/Mttp930 partially rescued the growth and photosynthesis-deficient phenotype of the mutant, and the chlorophyll content and light curve indicators could be restored to WT levels, indicating that the analyzed MtTP930-GFP was functional. The growth and photosynthesis phenotype of proMtTP930:MtTP930-GFP/Mttp930 could not be fully restored to WT levels, which may be due to the slight effect of the GFP tag on MtTP930 function (Supplementary Fig. S6). In conclusion, the fusion of GFP tag protein in the C-segment of MtTP930 is conducive to studying the function of MtTP930.

MtTP930, as a cargo sorting receptor for chloroplast protein, has both similarities and differences from traditional cargo

sorting receptors reported in animals, plants, and yeast (Contreras et al. 2004; Dancourt and Barlowe 2010; Geva and Schuldiner 2014; Barlowe and Helenius 2016). The similarity lies in the fact that these proteins act as cargo sorters during transport between the ER and the Golgi apparatus. Based on previous cell biology studies, some sorting receptors dynamically cycle between the COPII and COPI pathways due to their typical recognition motifs exposed to cytoplasm (Dancourt and Barlowe 2010; Gao et al. 2014). TANGO1, however, does not exit the ER, suggesting that shuttling back and forth is not a necessary characteristic of a cargo receptor itself (Saito et al. 2009). The typical motif PPP in MtTP930 might mediate the interaction with COPII components. It has been reported recently that PPP is a motif required for the interaction of the Tango1/cTAGE5 family with COPII components (Ma and Goldberg 2016; Peotter et al. 2019; Raote et al. 2020). Mutation of lysine residues leads to expression of the reporter protein on the cell surface in mammals (Nilsson et al. 1989; Jackson et al. 1990) and to its vacuolar delivery in yeast (Gaynor et al. 1994). Mutation of the KK motif of p24 caused its secretion to the prevacuolar compartment and the vacuole in plants (Langhans et al. 2008). However, we found that mutation of the KK motif resulted in an ERES localization of MtTP930 $^{\triangle KK}$, resembling the outcome observed after mutating the PPP motif. The function of the KK motif in cargo receptors may differ in plants compared to mammals and yeast, potentially leading to different

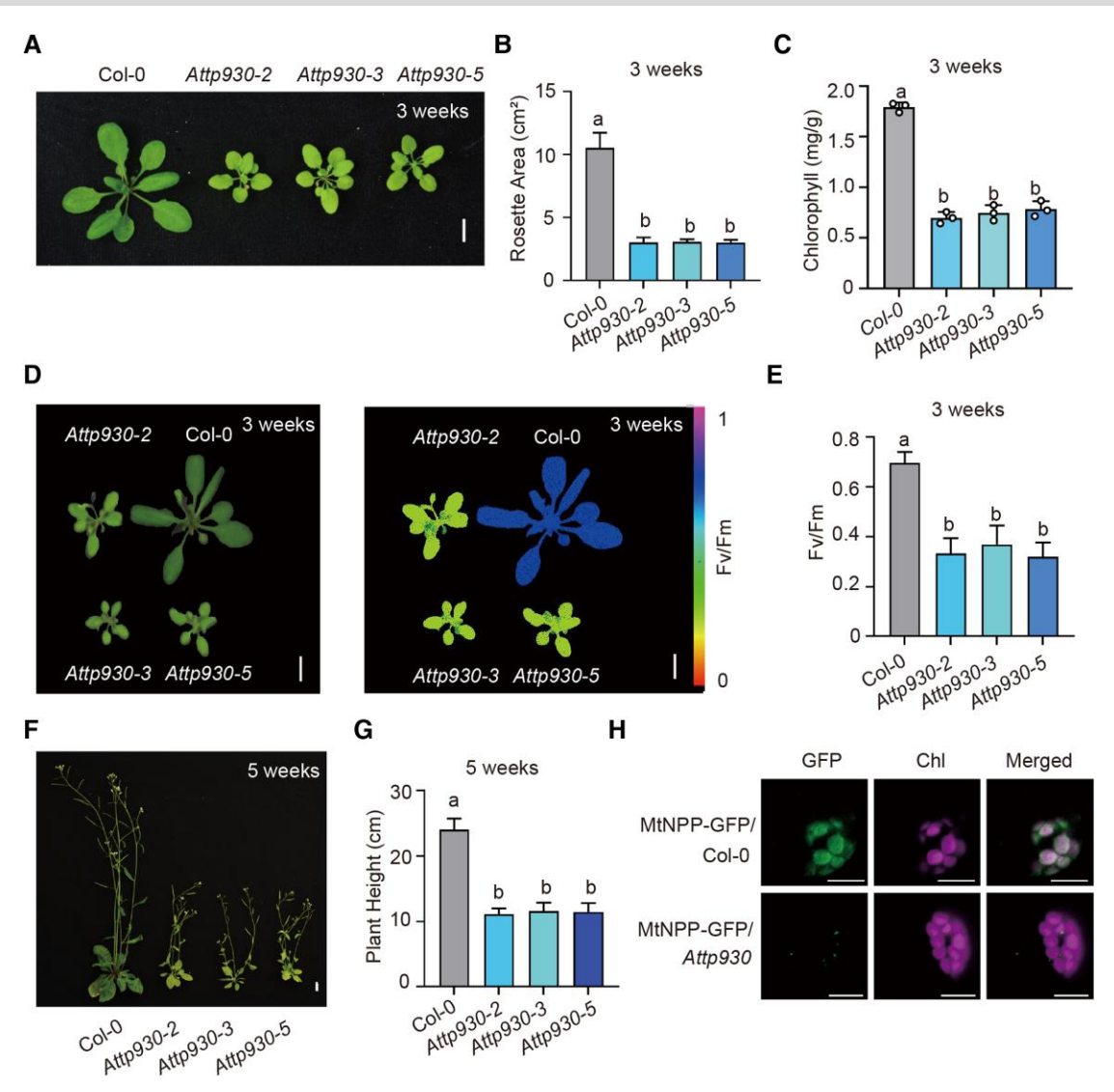


Figure 7. The function of MtTP930 is conserved in A. thaliana. A) Mutation of AtTP930 led to dwarf and photosynthetic defects. Morphological observation of the WT (Col-0), Attp930-2, Attp930-2, and Attp930-5 mutant plants grown under normal conditions for 3 wk. Scale bar, 1 cm. B and C) Rosette area and chlorophyll content of the Col-0, Attp930-2, Attp930-3, and Attp930-5 mutant plants grown for 3 wk under normal growth conditions. The data were shown as mean ± se, 1-way ANOVA, n > 15; significant differences are labeled (a, b, P < 0.05). D) Pictures (left panel) and PSII maximum quantum yield (F_w/F_m) false color images taken with the PlantExplorer (mobile chlorophyll fluorescence imaging system from PhenoTrait, right panel) of 3-wk-old Col-0, Attp930-2, Attp930-3, and Attp930-5 grown at normal growth conditions. Signal intensities for F_w/F_m are given by the false color scale. Scale bar, 1 cm. E) Bar graphs of the maximum quantum yield (F_w/F_m) of 3-wk-old Col-0, Attp930-2, Attp930-3, and Attp930-5 mutant plants. The data were shown as mean ± se, 1-way ANOVA, n > 15; significant differences are labeled (a, b, P < 0.05). F) Morphological observation of Col-0, Attp930-2, Attp930-3, and Attp930-5 mutant plants grown under normal conditions for 5 wk. Scale bar, 1 cm. G) The plant height of the 5-wk-old Col-0, Attp930-3, Attp930-3, and Attp930-5 mutant plants was measured. The data were shown as mean ± se, 1-way ANOVA, n > 15; significant differences are labeled (a, b, P < 0.05). H) Subcellular localization of MtNPP-GFP in Col-0 and Attp930 protoplasts. The MtNPP-GFP fusion protein driven by CaMV35S promoter (pE3025 vector) was transferred into the Arabidopsis mesophyll protoplasts. After a total of 16 h of transformation, fluorescence signals were observed using SP8 confocal microscope (Leica). Scale bars, 10 μm.

destinations for mutated proteins. The mechanism by which the mutations of KK and PPP affect the subcellular localization of MtTP930 remains to be further studied. We speculate that different cargo receptors are involved in the secretion pathway through a variety of motifs.

In our research, we have found that mutations in MtTP930 not only affect the trafficking of cargo proteins but may also affect their stability. We observed a notable decrease in the total protein content of MtNPP-GFP when expressed in the Mttp930 mutant genetic background (denoted as proMtNPP:MtNPP-GFP/Mttp930), as compared to its expression in the WT genetic background (designated as proMtNPP:MtNPP-GFP/WT; Fig. 5H), suggesting a potential mechanism in which the stability of MtNPP decreased in the

Mttp930 mutant. Therefore, additional research is warranted to ascertain the precise factors contributing to this reduction in protein content. MtCAH was localized in the vacuole in Mttp930 mutant protoplasts, which was quite different from that in the WT. We speculate that when MtNPP and MtCAH cannot be transported to chloroplasts by MtTP930, they may be degraded by different pathways. Therefore, MtTP930 is essential for the trafficking of its cargos, for example, MtNPP and MtCAH, to their proper destination.

Homologs of MtTP930 are widespread in green plants. We demonstrated the conservation of MtTP930 function through phenotypic analysis of the homolog Attp930 mutants in Arabidopsis (Fig. 7). While this work was under review, another 2 groups

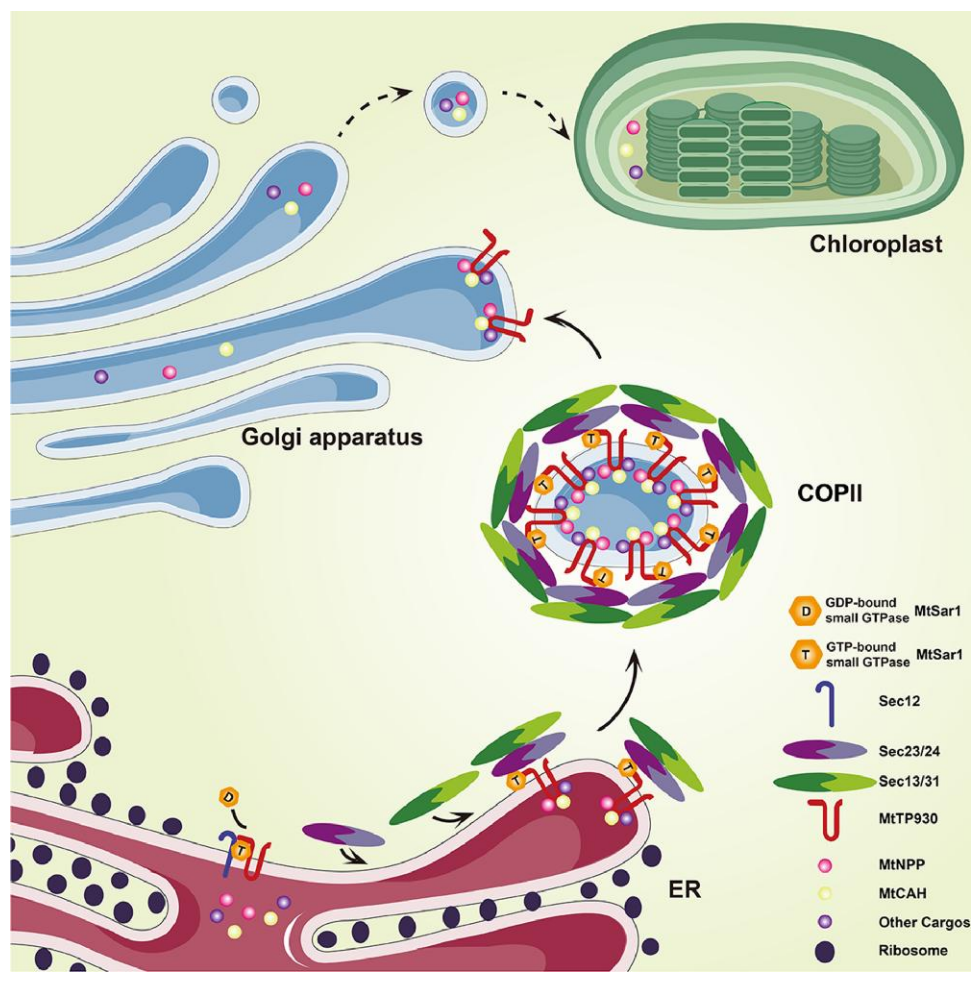


Figure 8. The working model of MtTP930. MtTP930 localizes in ERESs, recognizes cargo proteins MtNPP or MtCAH through the ER lumen region, and interacts with Sec12 through its N-terminal region. Sec12 then recruits Sar1 (small GTPase). After being catalyzed by Sec12, Sar1 is locally activated, exposes hydrophobic structures through GDP-GTP exchange, and inserts into the ER membrane. Then, Sar1 recruits the inner coat proteins Sec23/24, and Sec23/24 further recruit the outer coat proteins Sec13/31 to form the COPII vesicles. MtNPP, MtCAH, or other cargo proteins are loaded into COPII vesicles and transported to the Golgi apparatus.

reported the same protein as AtTP930, named DEAP2/FPB1 (Keller et al. 2023; Zhang et al. 2024). DEAP2 is involved in CP47 biogenesis (Keller et al. 2023). FPB1 and PAM68 synergistically integrate the last 2 CP47 TMDs and the connecting large loop into thylakoids and the PSII core during translation (Zhang et al. 2024). In this study, we discovered another function of the protein, which is as a cargo receptor that mediates the transport of a part of the nucleus-encoded chloroplast proteins to the chloroplast through the secretory pathway. This mechanism exhibits conservation across green plants.

Materials and methods Plant materials

M. truncatula plants used in this study are in the R108 background. The NF15872, NF7638, and NF18192 Tnt1 insertion mutants were identified in screens of lines from the Noble Research Institute and genetically characterized (Pislariu et al. 2012).

To generate the proMtTP930:MtTP930/NF15873 and proMtTP930: MtTP930/NF18192 lines, the 643-bp genomic sequence immediately upstream of the initiation codon (ATG) of MtTP930 was cloned and fused to the MtTP930 CDS in the pCAMBIA1381

backbone. The resulting construct was also transformed into the NF15873 and NF18192 mutants via the A. tumefaciens strain EHA105. proMtTP930:GUS was generated by cloning the promoter of MtTP930 and ligated into pCAMBIA1381. These constructs were transformed into R108 plants by A. tumefaciens strain EHA105. To generate the proMtTP930:MtTP930-GFP/Mttp930 plants, the promoter of MtTP930 was cloned and fused to the MtTP930 CDS and GFP tag in the pCAMBIA1381 backbone. The resulting construct was transformed into NF7638 and NF18192 via the A. tumefaciens strain EHA105.

To generate the proMtNPP:MtNPP-GFP/WT and prMtNPP:MtNPP-GFP/Mttp930 lines, the 2 kb genomic sequence immediately upstream of the initiation codon (ATG) of MtNPP was cloned and fused to the MtNPP-GFP in the pCAMBIA1381 backbone. The resulting construct was transformed into WT plants and Mttp930 (NF18192 and NF15873) mutants via the A. tumefaciens strain EHA105.

The generation of CRISPR-Attp930 mutant plants followed previously described procedures (Xing et al. 2014). The sgRNA cassettes targeting AtTP930 genes were amplified from pCBC-DT1T2 and then ligated into pHSE401 by the Golden Gate reaction. The ligation products were amplified in Escherichia coli and transferred into A. tumefaciens strain EHA105 for transformation of Arabidopsis

by the floral dipping transformation method (Clough and Bent 1998). The transgenic lines were identified by PCR, and the specific mutations were confirmed by sequencing.

Plant growth conditions

M. truncatula plants seeds were sterilized and grown as described previously (Zhu et al. 2020). M. truncatula plants used for extraction of protoplasts were grown in 1/2 MS agar culture bottles (pH 5.8). A. thaliana or N. benthamiana plant seeds were surface sterilized and germinated on 1/2 MS agar plates. The greenhouse conditions for M. truncatula, A. thaliana, and N. benthamiana were at 22 °C, 16-h light/8-h dark photoperiod, 70% to 80% humidity condition, and 70 to 100 μ mol/m²/s light intensity (Philips, TL-D 36W/ 865 1SL/25).

Phylogenetic analysis

To analyze the evolutionary relationships among MtTP930 and homologs from different species, the MtTP930 sequence and amino acid sequences from other species identified in the National Center for Biotechnology Information (NCBI, http://www.ncbi. nlm.nih.gov/) database were used to construct a phylogenetic tree using MEGA version 10/11 by the neighbor-joining method with 1,000 bootstrap replicates. Phylogenetic analysis of Sec12, Sar1, NPP, CAH, and Sec24 was conducted following the same approach as for MtTP930. Related files are provided as Supplementary Files S1 to S14.

Measurement of photosynthesis-related indicators

The photosynthetic rate was measured using the MINI-PAM-II instrument (Walz, Germany). After assembling the instrument according to the instructions, the leaves were clamped and observed for the Ft value. The Ft value was adjusted between 200 and 500 mV to keep an appropriate light intensity. The leaves were clamped with leaf clips and allowed to acclimate in the dark room for more than 15 min. The maximum quantum yield F_v/F_m was measured by inserting the fiber into the dark-adapted leaf clip, pulling out the slide, and clicking Fo, Fm. The photochemical light was turned on, and after the fluorescence value had stabilized (about 3 to 5 min), the "SAT" button was pressed to measure a set of actual quantum yields Y(II) at the corresponding light intensity. The following fluorescence-induced kinetic curve measurement parameters were used: illumination time width, 60 s; initial intensity, 3; and fast light curve step length, 8. The following light curve measurement parameters were used: the irradiation time for each light intensity gradient is greater than 30 s, usually 1 min; the initial intensity is 3; and the number of steps of the fast light curve (length) is generally 8. After the parameters were set, the corresponding data were measured.

Protein extraction and immunoblot analysis

To isolate the plant cell cytoplasm, membrane, and nucleus, MtTP930-Flag was transiently expressed in N. benthamiana via A. tumefaciens strain EHA105 and extracted as described previously (Lei et al. 2015). Briefly, N. benthamiana leaves expressing the target protein for 3 d after transformation were harvested and ground in liquid nitrogen. The membrane fraction, cytoplasm, and nuclear fraction were isolated as described (Du et al. 2015; Duan et al. 2017). The concentrations of the protein fraction were detected using a Coomassie (Bradford) protein assay kit. Each fraction was then analyzed by 10% (w/v) SDS-PAGE (with 1 mg of each fraction) and immunoblotted using the corresponding antibody: mouse monoclonal anti-Flag (Cat#F3165, Sigma-Aldrich; dilution: 1:10,000), rabbit polyclonal anti-Histone H3 (Cat#AS10710, Agrisera; dilution: 1:5,000), rabbit polyclonal anti-H+-ATPase (Cat# AS07260, Agrisera; dilution: 1:5,000), and rabbit polyclonal anti-cFBPase (Cat#AS04043, Agrisera; dilution: 1:5,000). Other antibodies used in this paper were as follows: rabbit polyclonal anti-BIP (Cat#AS09481, Agrisera; dilution: 1:2,000), mouse monoclonal anti-GFP (Cat#ab1218, Abcam; dilution: 1:5,000), mouse monoclonal anti-ACTIN (Cat# ab119952, Abcam; dilution: 1:5,000), mouse monoclonal anti-MYC (Cat#M4439-100UL, Sigma-Aldrich; dilution: 1:10,000), mouse monoclonal anti-HA (Cat#H3663-200UL, Sigma-Aldrich; dilution: 1:10,000), and rabbit anti-GUS (Cat#G5420-200UL, Sigma-Aldrich; dilution: 1:5,000).

Protease protection assay

N. benthamiana leaves expressing 35S:MtTP930-Flag were homogenized with extraction buffer (10 mm KCl, 1 mm MgCl₂, 0.4 mm sucrose, 0.4% [w/v] PVP, and 40 mm HEPES-KOH, pH 7.5) for 3 min. The samples underwent centrifugation at $1,000 \times q$ for 5 min at 4 °C, and the supernatants were subsequently transferred to a fresh tube kept on ice. A sucrose cushion was prepared in a 4-mL ultracentrifuge tube, consisting of 750 μ L of 20% (w/v) sucrose layered over 750 µL of 60% (w/v) sucrose, both dissolved in the extraction buffer. Lastly, 2 mL of the sample was gently added to the sucrose cushion and spun at 55,000 $\times g$ for 30 min at 4 °C. The microsomes were isolated, and the 100 µg/mL trypsin (Cat#9002-07-7, Sigma-Aldrich) was incubated at 30 °C for 2 h. Before adding trypsin and incubating at 30 °C for 30 min, the samples were pretreated with 1% (v/v) Triton X-100 on ice for 15 min. Then, the reaction was terminated as described (Ma et al. 2006; Sparkes et al. 2010). The samples were boiled for 10 min and then loaded on a 10% (w/v) SDS-PAGE gel. Immunoblot analysis was performed with mouse polyclonal anti-Flag (Cat#F3165, Sigma-Aldrich; dilution: 1:10,000) and rabbit anti-BIP antibodies (Cat#AS09481, Agrisera; dilution: 1:2,000).

Co-IP assay

The coding sequences of MtTP930, MtNPP, MtSar1, MtSec12, and MtSec24 were translationally fused downstream of the N-MYC tags or upstream of the GFP, HA, or Flag tags and cloned into pCAMBIA1307 binary vector, respectively. The constructed vectors were purified and transformed into Arabidopsis leaf protoplasts or N. benthamiana leaves. The protoplasts or N. benthamiana leaves were lysed using lysis and IP buffer (10 mm Tris-HCl pH 7.4, 150 mм NaCl, 10% [v/v] glycerin, 0.5% [v/v] NP-40, 2 mм PMSF [Coolaber], and 1 mm DTT [Solarbio]) and centrifuged ($100 \times g$, 3 min for protoplasts; $12,000 \times g$, 15 min for N. benthamiana leaves). The remaining supernatant was incubated with anti-GFP nanobody agarose beads (Cat#KTSM1338, AlpaLifeBio, 10 μL anti-GFP beads for combining with 15 to 20 μ g GFP-labeled fusion protein) at 4 °C for 3 h. After 2 to 5 washes in IP buffer, the Co-IP products were analyzed by immunoblot.

Immunofluorescence

The MtTP930 protein antibody used in the immunofluorescence experiment was a mouse-specific antibody against the small peptide fragment (SWAKPDSEEPPPWA), which was prepared by the BGI Company. Immunofluorescence labeling was performed according to a previously described method (Veiseth et al. 2011). The roots of 5-d-old M. truncatula seedlings were fixed with 4% (w/v) formaldehyde for 15 min and then flash frozen in liquid nitrogen. After treatment at 37 °C for 5 min, the samples were

washed with phosphate-buffered saline (PBS) solution (pH 7.4) 3 times. One percent (w/v) bovine serum albumin solution dissolved in PBS was added to block the sample for half an hour at 37 °C. The roots were incubated with mouse polyclonal anti-MtTP930 (dilution: 1:100), rabbit anti-ARF1 (Cat#AS08325, Agrisera; dilution: 1:1,000), or rabbit anti-Sar1 (Cat#AS08326, Agrisera; dilution: 1:50) antibodies, overnight at 4 °C for immunolabeling, and then were probed with mouse IgG-AF488 secondary antibody (Cat#QYB071, Qualityard; dilution: 1:500) and rabbit IgG-AF594 secondary antibody (Cat#QYB018, Qualityard; dilution: 1:500) for immunofluorescence detection by Leica SP8 laser scanning confocal system under a 100x confocal microscope. The relative fluorescence intensities shown in Fig. 2F were measured using the ImageJ software. The line or rectangular tool was selected from the toolbar, and the area indicated by the yellow line in the image was chosen for analysis using the ImageJ software. The horizontal axis denoted the pixel points along the line, while the vertical axis corresponded to the grayscale value of each point. The image illustrated the grayscale variation trend. By comparing the GFP/ RFP channel outcomes, the colocalization situation was reflected, and the data were then exported to Excel for redrawing.

Subcellular localization

To examine its subcellular localization, the MtTP930 ORF lacking a termination codon was inserted into the pE3025-RFP and p1300-GFP plasmid. Transformation of p1300-CaMV35S: MtTP930-GFP, pE3025-dCaMV35S:MtTP930-RFP, p1307-dCaMV35S: Sar1-GFP, pE3025-dCaMV35S:Sar1-GFP, and pNGFP-dCaMV35S: GFP-SYP32 into protoplasts of N. benthamiana, or cotransformation of pE3025-dCaMV35S:MtTP930-GFP with pE3025-dCaMV35S: MtNPP-GFP or pNGFP-dCaMV35S:MtCAH-GFP into protoplasts of M. truncatula, was performed as described previously (Jia et al. 2018). After 2- to 4-h BFA treatment, fluorescence signals were observed on a SP8 laser scanning confocal system under a laser confocal microscope. pE3025-dCaMV35S:MtNPP-GFP was transformed into the protoplasts of A. thaliana, as described (Yoo et al. 2007).

To investigate the subcellular localization of MtTP930, N. benthamiana leaves were transformed with p1300-CaMV35S: MtTP930-GFP, p1307-CaMV35S:RFP-Sec12, and p1307-CaMV35S: Sar1-RFP, as described (Du et al. 2015). The excitation wavelengths for GFP and RFP were precisely calibrated to 488 and 552 nm, respectively. Correspondingly, the GFP emission wavelengths captured fell within the range of 500 to 565 nm, whereas the RFP emission wavelengths encompassed the spectrum from 600 to 630 nm. Chloroplast autofluorescence was detected in the 650 to 720 nm range. Furthermore, the gain values underwent between 500 and 850. The relative fluorescence intensities were measured using the ImageJ software. The expression vectors used for the subcellular localization are listed in Supplementary Table S3.

BiFC assays

The PCR-amplified coding sequence of MtTP930 was introduced into pSPYNE(R) vectors, which contained the N-terminal (173 amino acid residue) part of eYFP. The coding sequences of MtSec12, MtSar1, and MtSec24 were individually introduced into pSPYCE (M), which contained the C-terminal (155 amino acid residues) region of eYFP. BiFC was performed in 4-wk-old N. benthamiana protoplasts. Fluorescence signals were observed using an SP8 laser scanning confocal system. The excitation wavelengths for YFP were precisely calibrated to 488 and 552 nm. The YFP emission wavelengths were within the range of 500 to 565 nm, and the gain values underwent between 500 and 850.

Firefly luciferase complementation assays

MtSec12, MtSar1, MtSec24, or MtNPP CDS was ligated to the C-terminal end of split Luc (p1300-CaMV35S:Cluc with stop codon was used to generate the target protein fused with Cluc at the C-terminus, and p1300-CaMV35S:Cluc without stop codon was used to generate the target protein fused with Cluc at the N-terminus), yielding p1300-CaMV35S:MtSec12-Cluc, p1300-CaMV35S:MtSar1-Cluc, p1300-CaMV35 S:MtSec24-Cluc, or p1300-CaMV35S:Cluc-MtNPP, respectively. MtTP930 CDS or truncated MtTP930 was ligated to the N-terminal end of split Luc yielding 1300-CaMV35S:MtTP930-Nluc, 1300-CaMV35 S:MtTP930n(1-125)-Nluc, 1300-CaMV35S:MtTP930c(140-181)-Nluc, and 1300-CaMV35S:MtTP930tm(103-162)-Nluc, respectively. Firefly luciferase (Luc) complementation imaging was performed according to the procedures described previously (Zhang et al. 2019). Briefly, each of the Cluc and Nluc constructs was transformed into N. benthamiana via A. tumefaciens strain EHA105. Subsequently, luciferin (560 μg/mL, Cat# E1602, Promega) was injected into N. benthamiana leaves expressing the target protein. The CCD imaging apparatus (CHEMIPROHT 1300B/LND, 16 bits; Roper Scientific) was used to visualize Luc activity.

SuY2H system

SuY2H was performed according to the manufacturer's instructions (Dualsystems Biotech p01001). MtTP930 was fused to Cub in pBT3-STE to generate BT3-STE-CYC1:MtTP930-Cub as a bait vector. pBT3-STE-CYC1:MtTP930-Cub, pPR3-C-ADH1:MtSec12-NubG, pPR3-C-ADH1:MtSec12-NubG, and pPR3-C-ADH1:NubG-MtNPP constructs were verified by DNA sequencing. Interactions were tested in yeast strain NMY51 on SD/-ade-his-leu-trp medium containing 15 mm 3-amino-1,2,4-triazole (3-AT). Transformants were incubated at 28 °C for 4 d. Alg5-NubI and Alg5-NubG with MtTP930-Cub were used as positive and negative controls, respectively.

GUS bioassays

To test the expression of GUS, proMtTP930:GUS transgenic seedlings were grown in pots of soil and watered with nitrogendepleted Fahräeus medium for 7 d and then inoculated with rhizobia (Sinorhizobium meliloti 1021; Sm1021). Samples were collected at 21 d postinoculation (dpi). The harvested material was stained with GUS staining solution (50 mm phosphate buffer [pH 7.0], 1 mm X-gluc, 5 mm potassium ferricyanide, and 5 mm potassium ferrocyanide), treated with a vacuum (>0.09 MPa) for 30 min, and then stained at 37 °C for 12 h (Cervera 2005). Overnight stained material was washed several times with 75% (v/v) ethanol and then imaged with an Olympus microscope system.

RNA extraction, RT-PCR, and RT-qPCR assays

Total RNA was extracted from M. truncatula or A. thaliana with TRIzol reagent (Invitrogen). Reverse transcription was performed with M-MLV reverse transcriptase (Promega). RT-PCR analysis was conducted by utilizing the 2XHieff PCR Master Mix (YEASEN, Cat#10102ES60). The process involved 34 cycles, with an annealing temperature set at 55 °C. Following the PCR, 18 μL of the product was analyzed via agarose gel electrophoresis. RT-qPCR analysis was performed in 3 biological replicates, and the expression of MtTP930 and AtTP930 were quantified using a CFX96 Real-Time PCR Detection System (Bio-Rad) and the $2^{-\Delta\Delta\text{CT}}$ method. MtACTIN, AtACT7, and AtUBQ5 were used as internal controls, respectively. Primers used for RT-PCR and RT-qPCR are listed in Supplementary Table S4.

Statistical analysis

GraphPad Prism (version 8.0) was used for data analysis. One-way ANOVA followed by Tukey's tests was used for pairwise multiple comparisons. A P < 0.05 was considered statistically significant. All detailed statistical analyses are shown in Supplementary Data Set 1

Accession numbers

Sequence data from this article can be found in the GenBank data libraries under the following accession numbers: MtTP930 (Medtr 7g095930), MtSar1 (Medtr7g112090), MtSec12 (Medtr4g084650), MtSec24 (Medtr7g111710), MtAERD2 (Medtr8g087430), MtRabE1d (Medtr1g068740), MtNPP (Medtr4g103520), MtCAH (Medtr1 g059960), OsNPP1 (AB100451.1), AtCAH1 (AT3G52720), AtSec12 (At2g01470), AtSar1 (At1g09180), AtSYP32 (At3g24350), and AtTP930 (At3g51510).

Acknowledgments

We thank Qijun Chen (College of Biological Science, China Agriculture University, China) for providing the CRISPR/Cas9 toolkit

Author contributions

J.D. and T.W. conceived and designed the experiments. J.L. and H.C. performed most of the experiments. L.L. constructed the Attp930 mutant and analyzed phenotypes. X.M. and Q.L. identified the Mttp930 mutant. J.W. provided the Mttp930 mutant materials. J.L. and H.C. wrote the manuscript. Q.Y., L.L., J.D., and T.W. revised the manuscript.

Supplementary data

The following materials are available in the online version of this article.

Supplementary Figure S1. Tissue expression pattern of MtTP930 in M. truncatula.

Supplementary Figure S2. Phylogenetic analysis of MtTP930 and its homologs from other species.

Supplementary Figure S3. MtTP930 interacted with COPII proteins.

Supplementary Figure S4. Nucleotide and amino acid sequences of MtNPP and MtCAH.

Supplementary Figure S5. Identification of MtTP930 homolog in A. thaliana.

Supplementary Figure S6. proMtTP930:MtTP930-GFP expression partially rescues growth and photosynthetic-deficient phenotypes of the mutants.

Supplementary Table S1. Genes associated with the Tnt1 insertion site of the NF15873 mutant.

Supplementary Table S2. Amino acid sequences of MtTP930. Supplementary Table S3. The expression vectors used in the

Supplementary Table S4. Primers used in this study.

Supplementary Data Set 1. Summary of statistical tests.

Supplementary Video S1. Time-lapse microscopy of MtTP930-GFP in the epidermal cells of N. benthamiana leaves. Monitored by SP8 laser scanning confocal system. Scale bar, 20 μm.

Supplementary File 1. Alignment of Sec12 in M. truncatula.

Supplementary File 2. Phylogenetic tree of Sec12 in M. truncatula.

Supplementary File 3. Alignment of Sar1 in M. truncatula.

Supplementary File 4. Phylogenetic tree of Sar1 in M. truncatula. **Supplementary File 5.** Alignment of Sec24 in M. truncatula.

Supplementary File 6. Phylogenetic tree of Sec24 in M.

Supplementary File 7. Alignment of NPP1 in M. truncatula. Supplementary File 8. Phylogenetic tree of NPP1 in M. truncatula.

Supplementary File 9. Alignment of CAH1 in M. truncatula.

Supplementary File 10. Phylogenetic tree of CAH1 in M. truncatula.

Supplementary File 11. Alignment of TP930 in different

Supplementary File 12. Phylogenetic tree of TP930 in different

Supplementary File 13. Alignment of TP930 in A. thaliana. Supplementary File 14. Phylogenetic tree of TP930 in A. thaliana.

Funding

This work was supported by the National Key Research and Development Program of China (2023YFF1001400), the Young Scientists Fund of the National Natural Science Foundation of China (32001391), the China Postdoctoral Innovative Talents Support Program (BX20190371), the China Postdoctoral Science Foundation (2019M660876), and the Faculty Resources Project of the College of Life Sciences, Inner Mongolia University (2022-101). Conflict of interest statement. None declared.

Data availability

The data underlying this article are available in the article and in its online supplementary material.

References

Asatsuma S, Sawada C, Itoh K, Okito M, Kitajima A, Mitsui T. Involvement of alpha-amylase I-1 in starch degradation in rice chloroplasts. Plant Cell Physiol. 2005:46(6):858-869. https://doi. org/10.1093/pcp/pci091

Bar-Peled M, Raikhel NV. Characterization of AtSEC12 and AtSAR1proteins likely involved in endoplasmic reticulum and Golgi transport. Plant Physiol. 1997:114(1):315-324. https://doi.org/10. 1104/pp.114.1.315

Barlowe C, Helenius A. Cargo capture and bulk flow in the early secretory pathway. Annu Rev Cell Dev Bi. 2016:32(1):197-222. https://doi.org/10.1146/annurev-cellbio-111315-125016

Béthune J, Wieland FT. Assembly of COPI and COPII vesicular coat proteins on membranes. Annu Rev Biophys. 2018:47(1):63-83. https://doi.org/10.1146/annurev-biophys-070317-033259

Cervera M. Histochemical and fluorometric assays for uidA (GUS) gene detection. Methods Mol Biol. 2005:286:203-214. https://doi. org/10.1385/1-59259-827-7:203

Chen MH, Huang LF, Li HM, Chen YR, Yu SM. Signal peptidedependent targeting of a rice alpha-amylase and cargo proteins to plastids and extracellular compartments of plant cells. Plant Physiol. 2004:135(3):1367–1377. https://doi.org/10.1104/pp.104. 042184

Cheng XF, Wang MY, Lee HK, Tadege M, Ratet P, Udvardi M, Mysore KS, Wen JQ. An efficient reverse genetics platform in the model

- legume Medicago truncatula. New Phytol. 2014:201(3):1065–1076. https://doi.org/10.1111/nph.12575
- Cheng XF, Wen JQ, Tadege M, Ratet P, Mysore KS. Reverse genetics in Medicago truncatula using Tnt1 insertion mutants. Plant Reverse Genetics: Methods Protocols. 2011:678:179–190. https://doi.org/10.1007/978-1-60761-682-5_13
- Chung KP, Zeng Y, Jiang L. COPII paralogs in plants: functional redundancy or diversity? *Trends Plant Sci.* 2016:21(9):758–769. https://doi.org/10.1016/j.tplants.2016.05.010
- Clough SJ, Bent AF. Floral dip: a simplified method for Agrobacterium-mediated transformation of Arabidopsis thaliana. Plant J. 1998:16(6):735–743. https://doi.org/10.1046/j.1365-313x. 1998.00343.x
- Contreras I, Yang YD, Robinson DG, Aniento F. Sorting signals in the cytosolic tail of plant p24 proteins involved in the interaction with the COPII coat. *Plant Cell Physiol.* 2004:45(12):1779–1786. https://doi.org/10.1093/pcp/pch200
- Dancourt J, Barlowe C. Protein sorting receptors in the early secretory pathway. Annu Rev Biochem. 2010:79(1):777–802. https://doi.org/10.1146/annurev-biochem-061608-091319
- De Craene JO, Courte F, Rinaldi B, Fitterer C, Herranz MC, Schmitt-Keichinger C, Ritzenthaler C, Friant S. Study of the plant COPII vesicle coat subunits by functional complementation of yeast Saccharomyces cerevisiae mutants. PLoS One. 2014:9(2): e90072. https://doi.org/10.1371/journal.pone.0090072
- Du JL, Zhang SW, Huang HW, Cai T, Li L, Chen S, He XJ. The splicing factor PRP31 is involved in transcriptional gene silencing and stress response in *Arabidopsis*. Mol Plant. 2015:8(7):1053–1068. https://doi.org/10.1016/j.molp.2015.02.003
- Duan M, Zhang R, Zhu F, Zhang Z, Gou L, Wen J, Dong J, Wang T. A lipid-anchored NAC transcription factor is translocated into the nucleus and activates Glyoxalase I expression during drought stress. Plant Cell. 2017:29(7):1748–1772. https://doi.org/10.1105/tpc.17.00044
- Forsythe ES, Williams AM, Sloan DB. Genome-wide signatures of plastid-nuclear coevolution point to repeated perturbations of plastid proteostasis systems across angiosperms. *Plant Cell*. 2021:33(4):980–997. https://doi.org/10.1093/plcell/koab021
- Gao CJ, Cai Y, Wang YJ, Kang BH, Aniento F, Robinson DG, Jiang LW. Retention mechanisms for ER and Golgi membrane proteins. Trends Plant Sci. 2014:19(8):508–515. https://doi.org/10.1016/j. tplants.2014.04.004
- Gaynor EC, te Heesen S, Graham TR, Aebi M, Emr SD. Signal-mediated retrieval of a membrane protein from the Golgi to the ER in yeast. *J Cell Biol.* 1994:127(3):653–665. https://doi.org/10.1083/jcb.127.3.653
- Geldner N, Denervaud-Tendon V, Hyman DL, Mayer U, Stierhof YD, Chory J. Rapid, combinatorial analysis of membrane compartments in intact plants with a multicolor marker set. *Plant J.* 2009:59(1):169–178. https://doi.org/10.1111/j.1365-313X.2009.03851.x
- Geva Y, Schuldiner M. The back and forth of cargo exit from the endoplasmic reticulum. *Curr Biol.* 2014:24(3):R130–R136. https://doi.org/10.1016/j.cub.2013.12.008
- Jackson MR, Nilsson T, Peterson PA. Identification of a consensus motif for retention of transmembrane proteins in the endoplasmic reticulum. EMBO J. 1990:9(10):3153–3162. https://doi.org/10.1002/j.1460-2075.1990.tb07513.x
- Jia N, Zhu Y, Xie F. An efficient protocol for model legume root protoplast isolation and transformation. Front Plant Sci. 2018:9:670. https://doi.org/10.3389/fpls.2018.00670
- Kaneko K, Takamatsu T, Inomata T, Oikawa K, Itoh K, Hirose K, Amano M, Nishimura S, Toyooka K, Matsuoka K, et al.

- N-Glycomic and microscopic subcellular localization analyses of NPP1, 2 and 6 strongly indicate that *trans*-Golgi compartments participate in the Golgi to plastid traffic of nucleotide pyrophosphatase/phosphodiesterases in rice. *Plant Cell Physiol.* 2016:57(8): 1610–1628. https://doi.org/10.1093/pcp/pcw089
- Keller JM, Frieboes MJ, Jodecke L, Kappel S, Wulff N, Rindfleisch T, Sandoval-Ibanez O, Gerlach I, Thiele W, Bock R, et al. Eukaryote-specific assembly factor DEAP2 mediates an early step of photosystem II assembly in Arabidopsis. Plant Physiol. 2023:193(3):1970–1986. https://doi.org/10.1093/plphys/kiad446
- Kitajima A, Asatsuma S, Okada H, Hamada Y, Kaneko K, Nanjo Y, Kawagoe Y, Toyooka K, Matsuoka K, Takeuchi M, et al. The rice alpha-amylase glycoprotein is targeted from the Golgi apparatus through the secretory pathway to the plastids. *Plant Cell*. 2009:21(9):2844–2858. https://doi.org/10.1105/tpc.109.068288
- Langhans M, Marcote MJ, Pimpl P, Virgili-Lopez G, Robinson DG, Aniento F. In vivo trafficking and localization of p24 proteins in plant cells. Traffic. 2008:9(5):770–785. https://doi.org/10.1111/j. 1600-0854.2008.00719.x
- Lei MJ, Wang Q, Li X, Chen A, Luo L, Xie Y, Li G, Luo D, Mysore KS, Wen J, et al. The small GTPase ROP10 of *Medicago truncatula* is required for both tip growth of root hairs and nod factor-induced root hair deformation. *Plant Cell*. 2015:27(3):806–822. https://doi.org/10.1105/tpc.114.135210
- Ma B, Cui ML, Sun HJ, Takada K, Mori H, Kamada H, Ezura H. Subcellular localization and membrane topology of the melon ethylene receptor CmERS1. Plant Physiol. 2006:141(2):587–597. https://doi.org/10.1104/pp.106.080523
- Ma W, Goldberg J. TANGO1/cTAGE5 receptor as a polyvalent template for assembly of large COPII coats. *Proc Natl Acad Sci U S A.* 2016:113(36):10061–10066. https://doi.org/10.1073/pnas. 1605916113
- Marti L, Fornaciari S, Renna L, Stefano G, Brandizzi F. COPII-mediated traffic in plants. *Trends Plant Sci.* 2010:15(9):522–528. https://doi.org/10.1016/j.tplants.2010.05.010
- Montesinos JC, Pastor-Cantizano N, Robinson DG, Marcote MJ, Aniento F. Arabidopsis p24 delta 5 and p24 delta 9 facilitate coat protein I-dependent transport of the K/HDEL receptor ERD2 from the Golgi to the endoplasmic reticulum. Plant J. 2014:80(6): 1014–1030. https://doi.org/10.1111/tpj.12700
- Nanjo Y, Oka H, Ikarashi N, Kaneko K, Kitajima A, Mitsui T, Munoz FJ, Rodriguez-Lopez M, Baroja-Fernandez E, Pozueta-Romero J. Rice plastidial N-glycosylated nucleotide pyrophosphatase/phosphodiesterase is transported from the ER-Golgi to the chloroplast through the secretory pathway. Plant Cell. 2006:18(10): 2582–2592. https://doi.org/10.1105/tpc.105.039891
- Nilsson T, Jackson M, Peterson PA. Short cytoplasmic sequences serve as retention signals for transmembrane proteins in the endoplasmic reticulum. *Cell.* 1989:58(4):707–718. https://doi.org/10. 1016/0092-8674(89)90105-0
- Peotter J, Kasberg W, Pustova I, Audhya A. COPII-mediated trafficking at the ER/ERGIC interface. *Traffic*. 2019:20(7):491–503. https://doi.org/10.1111/tra.12654
- Pislariu CI, Murray JD, Wen J, Cosson V, Muni RR, Wang M, Benedito VA, Andriankaja A, Cheng X, Jerez IT, et al. A *Medicago truncatula* tobacco retrotransposon insertion mutant collection with defects in nodule development and symbiotic nitrogen fixation. *Plant Physiol.* 2012:159(4):1686–1699. https://doi.org/10.1104/pp.112. 197061
- Radhamony RN, Theg SM. Evidence for an ER to Golgi to chloroplast protein transport pathway. *Trends Cell Biol.* 2006:16(8):385–387. https://doi.org/10.1016/j.tcb.2006.06.003

- Raote I, Chabanon M, Walani N, Arroyo M, Garcia-Parajo MF, Malhotra V, Campelo F. A physical mechanism of TANGO1-mediated bulky cargo export. *Elife*. 2020:9:e59426. https://doi.org/10.7554/eLife.59426
- Saito K, Chen M, Bard F, Chen S, Zhou H, Woodley D, Polischuk R, Schekman R, Malhotra V. TANGO1 facilitates cargo loading at endoplasmic reticulum exit sites. *Cell.* 2009:136(5):891–902. https://doi.org/10.1016/j.cell.2008.12.025
- Sibbald SJ, Archibald JM. Genomic insights into plastid evolution. Genome Biol Evol. 2020:12(7):978–990. https://doi.org/10.1093/gbe/evaa096
- Sjuts I, Soll J, Bolter B. Import of soluble proteins into chloroplasts and potential regulatory mechanisms. Front Plant Sci. 2017:8: 168. https://doi.org/10.3389/fpls.2017.00168
- Sparkes I, Tolley N, Aller I, Svozil J, Osterrieder A, Botchway S, Mueller C, Frigerio L, Hawes C. Five Arabidopsis reticulon isoforms share endoplasmic reticulum location, topology, and membrane-shaping properties. Plant Cell. 2010:22(4):1333–1343. https://doi.org/10.1105/tpc.110.074385
- Stefano G, Renna L, Chatre L, Hanton SL, Moreau P, Hawes C, Brandizzi F. In tobacco leaf epidermal cells, the integrity of protein export from the endoplasmic reticulum and of ER export sites depends on active COPI machinery. *Plant J.* 2006:46(1): 95–110. https://doi.org/10.1111/j.1365-313X.2006.02675.x
- Takeuchi M, Ueda T, Sato K, Abe H, Nagata T, Nakano A. A dominant negative mutant of Sar1 GTPase inhibits protein transport from the endoplasmic reticulum to the Golgi apparatus in tobacco and Arabidopsis cultured cells. *Plant J.* 2000:23(4):517–525. https://doi.org/10.1046/j.1365-313x.2000.00823.x
- Van Wijk KJ, Baginsky S. Plastid proteomics in higher plants: current state and future goals. *Plant Physiol*. 2011:155(4):1578–1588. https://doi.org/10.1104/pp.111.172932
- Veiseth SV, Rahman MA, Yap KL, Fischer A, Egge-Jacobsen W, Reuter G, Zhou MM, Aalen RB, Thorstensen T. The SUVR4 histone lysine methyltransferase binds ubiquitin and converts H3K9me1 to H3K9me3 on transposon chromatin in Arabidopsis. PLoS Genet. 2011:7(3):e1001325. https://doi.org/10.1371/journal.pgen. 1001325
- Villarejo A, Burén S, Larsson S, Déjardin A, Monné M, Rudhe C, Karlsson J, Jansson S, Lerouge P, Rolland N, et al. Evidence for a

- protein transported through the secretory pathway en route to the higher plant chloroplast. *Nat Cell Biol.* 2005:7(12):1224–1231. https://doi.org/10.1038/ncb1330
- Weigel AV, Chang CL, Shtengel G, Xu CS, Hoffman DP, Freeman M, Iyer N, Aaron J, Khuon S, Bogovic J, et al. ER-to-Golgi protein delivery through an interwoven, tubular network extending from ER. Cell. 2021:184(9):2412–2429. https://doi.org/10.1016/j.cell.2021. 03.035
- Xing HL, Dong L, Wang ZP, Zhang HY, Han CY, Liu B, Wang XC, Chen QJ. A CRISPR/Cas9 toolkit for multiplex genome editing in plants. BMC Plant Biol. 2014:14(1):327. https://doi.org/10.1186/s12870-014-0327-y
- Xu XM, Ouyang M, Lu DD, Zheng CH, Zhang LX. Protein sorting within chloroplasts. *Trends Cell Biol.* 2021:31(1):9–16. https://doi.org/10.1016/j.tcb.2020.09.011
- Yoo SD, Cho YH, Sheen J. Arabidopsis mesophyll protoplasts: a versatile cell system for transient gene expression analysis. Nat Protoc. 2007:2(7):1565–1572. https://doi.org/10.1038/nprot.2007.199
- Zeng Y, Chung KP, Li B, Lai CM, Lam SK, Wang X, Cui Y, Gao C, Luo M, Wong KB, et al. Unique COPII component AtSar1a/AtSec23a pair is required for the distinct function of protein ER export in Arabidopsis thaliana. Proc Natl Acad Sci U S A. 2015:112(46): 14360–14365. https://doi.org/10.1073/pnas.1519333112
- Zhang RX, Chen H, Duan M, Zhu FG, Wen JQ, Dong JL, Wang T. Medicago falcata MfSTMIR, an E3 ligase of endoplasmic reticulum-associated degradation, is involved in salt stress response. Plant J. 2019:98(4):680–696. https://doi.org/10.1111/tpj. 14265
- Zhang L, Ruan J, Gao F, Xin Q, Che LP, Cai L, Liu Z, Kong M, Rochaix JD, Mi H, et al. Thylakoid protein FPB1 synergistically cooperates with PAM68 to promote CP47 biogenesis and photosystem II assembly. Nat Commun. 2024:15(1):3122. https://doi.org/10.1038/s41467-024-46863-y
- Zhu F, Deng J, Chen H, Liu P, Zheng L, Ye Q, Li R, Brault M, Wen J, Frugier F, et al. A CEP peptide receptor-like kinase regulates auxin biosynthesis and ethylene signaling to coordinate root growth and symbiotic nodulation in *Medicago truncatula*. *Plant Cell*. 2020:32(9):2855–2877. https://doi.org/10.1105/tpc.20.00248